The ITCC-P4 PDX Platform Enables Preclinical Testing of Pediatric Cancers

Aniello Federico[1,2,3], Apurva Gopisetty[1,2,3], Didier Surdez[4,5,6], Yasmine Iddir[4,5,7], Robert J. Autry[1,2,3], Joshua J. Waterfall[4,5], Elnaz Saberi-Ansari[4,5,7], Charles Bobin[4,5,7], Stelly Ballet[8], Gaelle Pierron[8], Justyna A. Wierzbinska[9], Andreas Schlicker[9], Martin Sill[1,2,3], Richard Volckmann[10], Danny A. Zwijnenburg[10], Alan Mackay[11], Sakina Zaïdi[4,5], Alexandra Saint-Charles[4,5,7], Norman Mack[1,2,3], Benjamin Schwalm[1,2,3], Sebastian Brabetz[1,2,12], Lena Weiser[13], Ivo Buchhalter[13], Christopher Previti[1,2,13], Anna-Lisa Böttcher[1,2,3], Fatima Iradier[14], Eva-Maria Rief[15], David T.W. Jones[1,2,3], Olaf Witt[1,2,3], Frank Westermann[1,2,3], Till Milde[1,2,3,16], Angelika Eggert[17], Nicole Huebener[17], Johannes H. Schulte[17,18], Sara Colombetti[19], Louis Chesler[11], Elizabeth R. Tucker[11], Alaide Morcavallo[11], Federica Lorenzi[11], Heinrich Kovar[20], Jan-Henning Klusmann[21], Klaus-Michael Debatin[22], Simon Bomken[23], Christina D. Guttke[24], Petra Hamerlik[25], Maureen M. Hattersley[26], Michelle Garcia[27], Frédéric Colland[28], Ashley Strougo[29], Pablo Aviles[30], Michal Zapotocky[31], David Sumerauer[31], Johannes Gojo[1,2,3,32], Walter Berger[33], Daniela Lötsch-Gojo[34], Julia Schueler[35], Emily J. Girard[36], James M. Olson[36], Beat W. Schäfer[37], Marco Wachtel[37], Jan J. Molenaar[38], Biljana Dumevska[39], Elisabet Fernandez Potente[40], Chris Jones[11], Angel M. Carcaboso[41], Emilie Indersie[42], Stefano Cairo[42], Katia Scotlandi[43], Maria Cristina Manara[43], Lorena Landuzzi[43], Angela Di Giannatale[44], Patrizia Gasparini[45], Massimo Moro[45], Dennis Gürgen[46], Jens Hoffmann[46], Maria Eugenia Marques da Costa[47], Birgit Geoerger[47], Olivier Delattre[4,5], David J. Shields[48], Hubert N. Caron[19], Gilles Vassal[15,47,49], Louis F. Stancato[14,50], Stefan M. Pfister[1,2,3,15,49,51], Natalie Jäger[1,2,3], Jan Koster[10], Marcel Kool[1,2,3,38,52], and Gudrun Schleiermacher[4,5,7]

ABSTRACT

Cancer is the leading cause of disease-related deaths among children in high-income countries. Tumor heterogeneity and the lack of mechanism of action–based therapeutic options are key challenges to overcome to improve the survival of pediatric patients with cancer. To address these challenges, we formed the European Union-Innovative Medicines Initiative 2 (EU-IMI2) funded public–private partnership "Innovative Therapies for Children with Cancer Paediatric Preclinical Proof-of-Concept Platform" (ITCC-P4), which built a large repertoire of patient-derived xenograft (PDX) models representing all major high-risk solid pediatric cancer types for *in vivo* drug testing. A total of 353 PDX models were established from diagnostic and relapsed pediatric cancers and molecularly characterized, together with matched germline/tumor samples. Serial PDX models were also established, spanning diagnostic/posttreatment, primary/relapse, and metastasis-derived pairs. Proof-of-concept *in vivo* drug screening data in neuroblastoma and rhabdomyosarcoma models identified potential predictive biomarkers for targeted therapy. Molecular data from the PDX models, accessible at https://r2platform.com/itcc-p4, allowed the selection of models for preclinical testing based on oncogenic drivers and/or potential biomarkers. Operated by a nonprofit entity, this sustainable platform aids academic and industrial researchers in developing and prioritizing innovative therapies for pediatric cancer.

Significance: The ITCC-P4 platform comprises models of diagnostic/refractory/relapsed pediatric cancers that mimic patient tumors and feature intertumoral heterogeneity, providing a resource of molecularly characterized patient-derived models for *in vivo* testing.

[1]Hopp Children's Cancer Center (KiTZ), Heidelberg, Germany. [2]German Cancer Research Center (DKFZ), German Cancer Consortium (DKTK), Heidelberg, Germany. [3]National Center for Tumor Diseases (NCT), Heidelberg, Germany. [4]INSERM U1330, Childhood Oncology Research Unit (CONCERT), Institut Curie, Paris, France. [5]SIREDO Pediatric Oncology Centre (Care, Innovation and Research for Children, Adolescents and Young Adults with Cancer), Institut Curie Research Centre, PSL Research University, Paris, France. [6]Balgrist University Hospital, Faculty of Medicine, University of Zürich (UZH), Zürich, Switzerland. [7]RTOP (Recherche Translationelle en Oncologie Pédiatrique), Translational Research Department, Institut Curie Research Center, PSL Research University, Institut Curie, Paris, France. [8]Unité de Génétique Somatique, Département de Génétique, Institut Curie, Paris, France. [9]Research & Development, Pharmaceuticals, Bayer AG, Berlin, Germany. [10]Center for Experimental and Molecular Medicine, Laboratory of Experimental Oncology and Radiobiology, Cancer Center Amsterdam, Amsterdam UMC, University of Amsterdam, Amsterdam, the Netherlands. [11]Division of Clinical Studies, The Institute of Cancer Research, London, United Kingdom. [12]Champions Oncology, Neu Ulm, Germany. [13]Core Facility Omics IT and Data Management (ODCF), German Cancer Research Center (DKFZ), Heidelberg, Germany. [14]Eli Lilly and Company, Indianapolis, Indiana. [15]ITCC-P4 gGmbH, Heidelberg, Germany. [16]Department of Pediatrics and Adolescent Medicine, Jena University Hospital, Friedrich Schiller University Jena, Jena, Germany. [17]Department of Pediatric Oncology/Hematology, Charité-Universitätsmedizin Berlin, Berlin, Germany. [18]Department of Pediatric Hematology, Oncology, Gastroenterology, Nephrology and Rheumatology, University Hospital Tübingen, Tübingen, Germany. [19]Hoffman-La Roche, Basel, Switzerland. [20]Children's Cancer Research Institute, St Anna Kinderkrebsforschung, Vienna, Austria.

Downloaded from aacrjournals.org/cancerres/article-pdf/86/19/4755/3830682/can-25-5295.pdf by DKFZ - German Cancer Research Center user on 17 November 2026

Introduction

Cancer represents the leading cause of disease-related death in childhood in high-income countries [World Health Organization (WHO); ref. 1]. Pediatric cancers are characterized by embryonal origins, a relatively low mutational burden, high intertumoral heterogeneity, and cellular plasticity (2–7). The most frequent types are acute leukemias and lymphomas, followed by central nervous system (CNS) tumors and solid extracranial tumors, including neuroblastoma, soft-tissue sarcoma, and bone sarcoma (1).

Despite advances in pediatric cancer research, the lack of effective novel therapeutic options for patients with high-risk disease or treatment failure has hampered survival improvements over the past few decades. Furthermore, most childhood cancer survivors experience long-term treatment-related sequelae. Targetable molecular alterations identified in precision medicine programs have led to effective treatments in only a minority of cases, and coordinated, multidisciplinary approaches are required to accelerate drug development for children with cancer (8–13). Patient-derived xenografts (PDX) are currently regarded as the most predictive preclinical models for evaluating new drugs and investigating treatment resistance mechanisms *in vivo*. They preserve the main molecular features of original tumors, and PDX treatment responses have been shown to correlate with those observed in patients (14–20).

However, large collections of molecularly well-characterized pediatric PDX models accessible for commercial drug testing remain lacking, limiting their utility for developing innovative pediatric therapies (15, 17, 21–26). Key challenges for pediatric PDX cohorts include covering the full spectrum of molecular subtypes and intra-/intertumoral heterogeneity; including models from treatment-naïve and treatment-resistant states; integrating molecular data from PDXs with patient tumor and germline molecular data; operating standardized workflows bridging academic and industry gaps; and enabling broad access for preclinical drug testing. To address these objectives, a public–private partnership was formed in 2017 as the "Innovative Therapies for Children with Cancer Paediatric Preclinical Proof-of-Concept Platform" (ITCC-P4), which in 2023 transitioned into a nonprofit company (www.itccp4.com). Here, we describe the first 353 fully established and extensively characterized PDX models representing a diverse spectrum of high-risk pediatric malignancies, including 189 models (54%) from refractory or relapsed disease, supported by comprehensive multiomics characterization and *in vivo* drug testing results.

Materials and Methods

Patient sample collection

Patient-derived material and clinical data were collected under institutional ethical approval (University of Heidelberg and collaborating centers) and in accordance with the Declaration of Helsinki. Written informed consent was obtained from all patients or their legal guardians. Tumor and matched germline samples were collected as part of the MAPPYACTS study (9) and/or collaborating ITCC-P4 sites. Detailed information on patient enrollment, sample collection, written consent procedures, and data management is provided in the Supplementary Methods.

PDX model establishment

All animal procedures complied with institutional and European guidelines (Directive 2010/63/EU). All experiments were reviewed and approved by the appropriate institutional animal ethics committees and competent national authorities at each participating center. Fresh tumor tissues from patients were implanted into immunodeficient mice to generate PDX models. Orthotopic models were established for brain tumors and subcutaneous models for non-brain tumors, following approved analgesia and anesthesia protocols. PDX tumors were expanded across passages and cryopreserved for molecular characterization and biobanking. Detailed

[21]Department of Pediatrics, Martin-Luther-University Halle-Wittenberg, Halle, Germany. [22]Department of Pediatrics and Adolescent Medicine, Ulm University Medical Center, Ulm, Germany. [23]Translational and Clinical Research Institute, Newcastle University, The Great North Children's Hospital, Newcastle upon Tyne, United Kingdom. [24]Janssen Research & Development, LLC, Spring House, Pennsylvania. [25]AstraZeneca, R&D, Cambridge, United Kingdom. [26]AstraZeneca, R&D, Waltham, Massachusetts. [27]Amgen, Los Angeles, California. [28]Institut de Recherches Servier, Croissy-sur-Seine, France. [29]Sanofi-Aventis Deutschland GmbH, R&D, Frankfurt, Germany. [30]PharmaMar S.A., Madrid, Spain. [31]Department of Paediatric Haematology and Oncology, Second Faculty of Medicine, Charles University, University Hospital Motol, Prague, Czech Republic. [32]Department of Pediatrics and Adolescent Medicine, Comprehensive Center for Pediatrics and Comprehensive Cancer Center, Medical University of Vienna, Vienna, Austria. [33]Center of Cancer Research and Comprehensive Cancer Center, Medical University of Vienna, Vienna, Austria. [34]Department of Neurosurgery, Medical University of Vienna, Vienna, Austria. [35]Charles River Discovery Research Services Germany, Freiburg, Germany. [36]Seattle Children's and University of Washington, Seattle, Washington. [37]Department of Oncology, Children's Research Center, University Children's Hospital, Zürich, Switzerland. [38]Princess Máxima Center for Pediatric Oncology, Utrecht, the Netherlands. [39]Children's Cancer Institute Australia, Institute of Technology, Sydney, Australia. [40]Division of Molecular Pathology, Institute of Cancer Research, London, United Kingdom. [41]SJD Pediatric Cancer Center Barcelona, Hospital Sant Joan de Déu Barcelona, Institut de Recerca Sant Joan de Deu, Barcelona, Spain. [42]Xentech, Evry-Courcouronnes, France. [43]Laboratory of Oncology Research and Functional Genomics (ONCOGEN), IRCCS Istituto Ortopedico Rizzoli, Bologna, Italy. [44]Department of Pediatric Hematology/Oncology and Cell and Gene Therapy, IRCCS, Ospedale Pediatrico Bambino Gesù, Rome, Italy. [45]Fondazione IRCCS Istituto Nazionale dei Tumori di Milano, Milan, Italy. [46]Experimental Pharmacology and Oncology (EPO) Berlin-Buch GmbH, Berlin, Germany. [47]Gustave Roussy Cancer Campus, Department of Pediatric and Adolescent Oncology, INSERM U1015, Université Paris-Saclay, Villejuif, France. [48]Pfizer Centers for Therapeutic Innovation, Pfizer Inc., New York, New York. [49]European Consortium for Innovative Therapies for Children with Cancer (ITCC), Paris, France. [50]Indiana Biosciences Research Institute, Indianapolis, Indiana. [51]Department of Pediatric Hematology and Oncology, Heidelberg University Hospital, Heidelberg, Germany. [52]Utrecht University Medical Center, Utrecht University, Utrecht, the Netherlands.

A. Federico, A. Gopisetty, and D. Surdez contributed equally to this article.

J. Koster, M. Kool, and G. Schleiermacher contributed equally to this article.

Lead contact: G. Schleiermacher.

Corresponding Authors: Marcel Kool, Princess Máxima Center for Pediatric Oncology, Heidelberglaan 25, Utrecht 3584 CS, the Netherlands. E-mail: m.kool-5@prinsesmaximacentrum.nl; and Gudrun Schleiermacher, SIREDO Pediatric Oncology Center, Laboratory of Translational Research in Pediatric Oncology – INSERM U1330, Institut Curie, 26 rue d'Ulm, Paris Cedex 05 75248, France. E-mail: gudrun.schleiermacher@curie.fr

Cancer Res 2026;86:4755–71

doi: 10.1158/0008-5472.CAN-25-5295

This open access article is distributed under the Creative Commons Attribution-NonCommercial-NoDerivatives 4.0 International (CC BY-NC-ND 4.0) license.

©2026 The Authors; Published by the American Association for Cancer Research

Downloaded from aacrjournals.org/cancerres/article-pdf/86/19/4755/3830682/can-25-5295.pdf by DKFZ - German Cancer Research Center user on 17 November 2026

procedures for tumor dissociation, transplantation, animal care, monitoring, and reimplantation are described in the Supplementary Methods.

Nucleic acid extraction

DNA and RNA were extracted from tissue samples using automated purification systems and standardized protocols. Nucleic acid yield and integrity were assessed by fluorometric quantification and electrophoretic analysis, with RNA samples meeting a minimum integrity RNA integrity number (RIN) threshold of ≥7. Details of extraction kits, instrumentation, and quality control procedures are provided in the Supplementary Methods.

ITCC-P4 barcoding system

Human and PDX samples, along with associated clinical and molecular data, were anonymized and tracked using an automated barcoding system. Details of the coding structure and data registration process are provided in the Supplementary Methods.

Molecular profiling and data processing

Whole-genome and whole-exome sequencing workflow

Patient and PDX tumor samples underwent library preparation and sequencing at two ITCC-P4 partner sites [German Cancer Research Center (DKFZ) and Institut Curie] using low-coverage whole-genome sequencing (lcWGS) and whole-exome sequencing (WES). Additional raw sequencing data were obtained from collaborating institutions. To assess species composition in PDX-derived DNA sequencing libraries, reads were classified as graft (human)- or host (mouse)-assigned using xengsort. Sequencing reads were then aligned to a combined human-mouse reference genome, and variant calling was performed using standardized in-house pipelines. Full details of library preparation, sequencing platforms, and bioinformatics workflows are provided in the Supplementary Methods.

Processing samples without patient-matched germline data (no-control workflow)

For PDX samples lacking matched germline controls, variant detection was performed using an established in-house "no-control" workflow integrating multiple variant calling tools. Common germline variants were excluded using population and reference databases, and functional annotation and filtering were conducted to prioritize rare, potentially pathogenic variants. Detailed pipeline configurations and filtering parameters are provided in the Supplementary Methods.

DNA methylation profiling and analysis

Genomic DNA from patient tumors and matched PDX samples was profiled using Illumina Methylation 450K and EPIC BeadChip arrays at DKFZ and Institut Curie. Data processing, normalization, and quality control were performed using the RnBeads Bioconductor (RRID:SCR_010958; RRID:SCR_006442) package. Tumor classification and molecular subtype assignment were based on established DNA methylation classifiers and unsupervised clustering analyses. Full preprocessing parameters, filtering criteria, and classifier references are described in the Supplementary Methods.

Copy-number variation analysis

Copy-number variations (CNV) in patient tumors and PDX models were characterized using multiple complementary computational tools, including ichorCNA, Sequenza (RRID:SCR_016662), CNVkit, and conumee, to ensure accurate detection of large-scale and focal copy-number alterations and reliable tumor purity estimation. Sequencing- and methylation-based approaches were combined to provide a comprehensive CNV profile. Full details of pipelines, parameters, and input requirements are provided in the Supplementary Methods.

RNA sequencing and analysis

RNA sequencing (RNA-seq) of patient tumors and PDX models was performed on Illumina HiSeq instruments. Data were processed using the established DKFZ One Touch Pipeline in-house RNA-seq workflow (based on the Roddy framework), including read alignment with STAR (RRID:SCR_004463), gene expression quantification with featureCounts (RRID:SCR_012919), and gene fusion detection with Arriba. Processed expression data were used for unsupervised clustering, differential gene expression, and Gene Ontology analyses. Full details of pipeline versions, parameters, and downstream analyses are provided in the Supplementary Methods.

Identification and annotation of driver genes for mutational landscape analysis

Driver genes were identified and annotated using curated references, including the 2022 WHO Classification of Pediatric Tumors and published reviews on pediatric solid cancers. Tumor mutational burden (TMB) was calculated from high-confidence coding single-nucleotide variants (SNV) and insertions/deletions (indel) derived from WES. Variant allele frequencies (VAF) were computed to assess intratumor heterogeneity and clonal evolution in PDX models. PDX-tumor correlations were further evaluated using metrics such as deltaVAF and VAF ratios. Statistical analyses, including correlation and fold change calculations, were performed in R.

We aimed to identify and annotate important driver genes for the analysis of the mutational landscape. To accomplish this, we relied on two key references: the 2022 WHO Classification of Pediatric Tumors (6) and a published review by Jones and colleagues (27) focusing on pediatric solid cancers to curate a comprehensive list of known somatic and germline driver mutations.

To prioritize functionally and clinically relevant SNVs, we then focused on a curated set of known tumor type–specific driver genes, selected based on their involvement in tumorigenesis and their potential as therapeutic targets (28, 29). The full reports of annotated variants (called with the hg19 assembly) for each model are available on our public platform ITCC-P4 Data Scope in R2 (https://r2platform.com/itcc-p4) upon request.

Analysis of TMB

TMB (30) was calculated for the ITCC-P4 samples based on SNVs and small indels determined by WES data, focusing on the coding regions targeted by the respective WES library preparation kits. Only high-confidence, somatic, and functional exonic SNVs and indels were considered for TMB calculation. The obtained results were compiled and utilized for comparing the mutation load between matched PDX–tumor pairs across different cancer subgroups, disease states, and model types (paired Wilcoxon test).

Calculation of VAF

To gain insights into clonal selection, the distinction between somatic and germline variants, and the evolution within the PDX samples, we performed calculations to determine the VAF of functional somatic SNVs. The first step involved extracting the DP4 values from the aligned and processed somatic functional SNV

Downloaded from aacrjournals.org/cancerres/article-pdf/86/19/4755/3830682/can-25-5295.pdf by DKFZ - German Cancer Research Center user on 17 November 2026

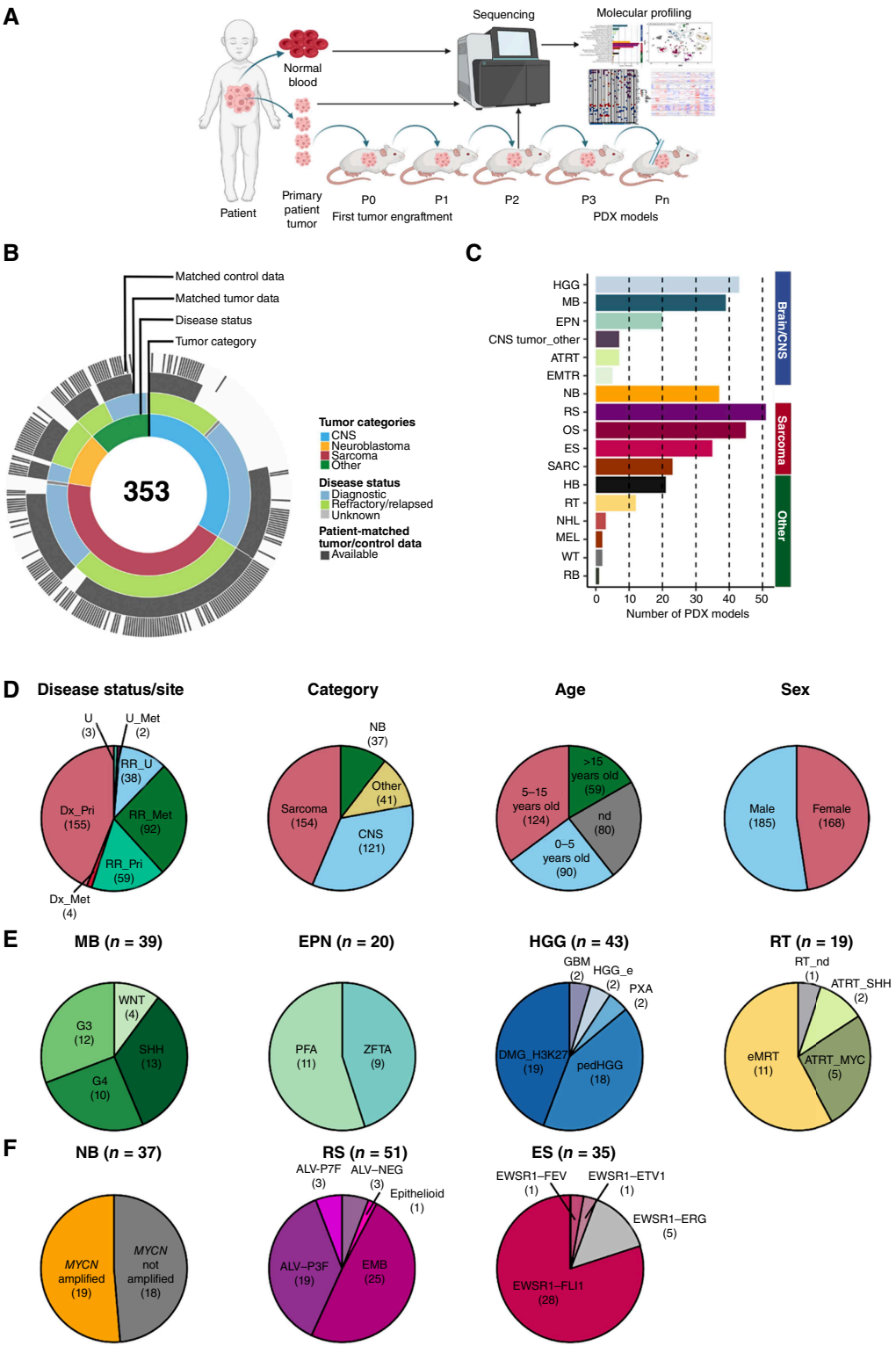


Figure 1.

ITCC-P4 PDX models: pipeline and cohort overview. **A,** Schematic representation of PDX establishment and molecular characterization. Tumors obtained from pediatric patients with cancer were first injected into mice (first passage, P0); following two mouse-to-mouse passages (P1 and P2), the PDX models were considered established. Multiomics profiling of established PDX models and matching patient material (tumor, blood) included DNA methylation, lcWGS, high-coverage WES, RNA-seq, and Affymetrix gene expression profiling. PDX tumor material harvested in the following (*Continued on the following page.*)

Downloaded from aacrjournals.org/cancerres/article-pdf/86/19/4755/3830682/can-25-5295.pdf by DKFZ - German Cancer Research Center user on 17 November 2026

files. The DP4 value represents the sequencing depth for each allele (reference and alternate) in each sample and is commonly used to indicate the number of reads supporting each allele. It comprises four subfields that indicate the coverage of the reference allele by forward reads, the coverage of the reference allele by reverse reads, the coverage of the alternate allele by forward reads, and the coverage of the alternate allele by reverse reads. Subsequently, the VAF scores were calculated using the following formula:

$$\text{VAF} = (\text{forward non-ref allele} + \text{reverse non-ref allele})/(\text{forward ref} + \text{reserve ref} + \text{forward non-ref} + \text{reverse non-ref})$$

PDX-tumor correlation analysis using deltaVAF and VAF ratios

In order to assess and establish the correlation of clonal discordance between the VAFs of tumors and PDX models, we introduced a metric called "deltaVAF." This metric was derived by subtracting the tumor VAF from the PDX VAF. The identification of PDX-specific variants within a sample played a crucial role in the investigation of significant subclones. To analyze the presence of overlapping or exclusive variants between PDX and tumor, we introduced another metric known as "VAFratio." The VAFratio scores were calculated by summing the PDX VAF and dividing it by the sum of the tumor VAF for each patient sample, facilitating a quantitative comparison of variant frequencies.

Clonal evolution analysis

Clonal evolution analysis was performed using PyClone (RRID: SCR_016873) to infer cancer cell fractions (CCF) from allelic count data, integrating total copy number and tumor purity estimates obtained with Sequenza or iChorCNA for each somatic SNV. A β-binomial distribution was used as the statistical model, with 10 random restarts. Clonal ordering was inferred using the clonevol R package under a monoclonal model, with subclonal structure assessed by nonparametric bootstrapping (1,000 iterations). The founding clone was defined as the cluster with the highest initial CCF, using a minimum CCF threshold of 0.001. Clonal architectures were visualized using fish plots generated from ClonEvol output. For copy-number estimates derived from ichorCNA, allelic copy numbers were not directly available. We applied a simplifying assumption to infer allelic major and minor copy numbers from the total copy number:

$$\text{Total CN} = 1 \rightarrow \text{allelic minor CN} = 0 \text{ and allelic major CN} = 1$$

$$\text{Total CN} \geq 2 \rightarrow \text{allelic minor CN} = 1 \text{ and allelic major CN} = \text{total CN} - \text{allelic minor CN}$$

The total copy number was capped at five, limiting the maximum copy number considered in the analysis.

In vivo drug treatment studies in PDX models

PDX model expansion for *in vivo* drug testing was performed by contract research organizations [CRO; Charles River, Experimental Pharmacology and Oncology (EPO), and Xentech] according to standardized protocols. Treatment was initiated when tumors reached predefined size criteria, determined either by caliper measurement for subcutaneous models or by bioluminescence imaging for orthotopic CNS models.

For proof-of-principle *in vivo* testing, selected ITCC-P4 PDX models were treated using an $n = 1$ single-mouse trial design (26, 31). The following treatment regimens were used: etoposide, 5 mg/kg, intravenously, once daily, 5 days on/2 days off for 3 weeks; idasanutlin, 100 mg/kg, orally, twice daily, 5 days on/2 days off for 4 weeks; JQ-1, 50 mg/kg, intraperitoneally, once daily, 5 days on/2 days off for 4 weeks; topotecan, 0.5 mg/kg, intravenously, once daily, 5 days on/2 days off; prexasertib, 10 mg/kg, subcutaneously, twice daily, 3 days on/4 days off for 3 weeks; cobimetinib, 7.5 mg/kg, orally, once daily, 21 days within a 28-day period; lorlatinib, 3 mg/kg, orally, twice daily for 28 days; copanlisib, 10 mg/kg, intravenously, 2 days on/5 days off; cisplatin plus cyclophosphamide, 2 mg/kg cisplatin, intravenously, every 7 days for 4 doses, followed by 100 mg/kg cyclophosphamide, intraperitoneally, every 7 days for 4 doses, administered 1 day later; and vincristine plus actinomycin D, 0.5 mg/kg vincristine intravenously every 5 days for 6 doses plus 0.5 mg/kg actinomycin D intravenously every 7 days for 4 doses, administered 1 day later. In each experiment, treatment groups were compared with a vehicle control group ($n = 3$) administered orally twice daily for 28 days.

Statistical analysis

All statistical calculations (such as Pearson correlation and $\log_2$ fold change values) and downstream molecular analyses for this study were conducted, and graphical visualizations were generated within the R environment.

Results

The ITCC-P4 PDX platform

Fresh patient-derived tumor samples were collected at ITCC-P4 partner sites and transplanted into immunodeficient (NOD/SCID gamma, Swiss-Nude, or CB17-SCID) mice. The focus has been on high-risk tumor types only, as low-risk tumors do not engraft or do so only with very low success rates (Supplementary Fig. S1A). CNS tumor samples were injected orthotopically, whereas non-brain tumors were transplanted subcutaneously. Established PDX tumors were propagated through at least three passages (i.e., ≥P2), and tumor fragments from established PDX models were processed for molecular characterization together with matching patient tumors and germline material (**Fig. 1A**; Supplementary Fig. S1B).

The 353 established PDX models originate from diagnostic (159; 45%), refractory/relapsed (189; 54%), or unknown (5; 1%) high-risk

(*Continued.*) xenopassages (P2 and higher) either supplies the ITCC-P4 PDX biobank or is used for downstream applications (drug testing, *in vitro* cultures, etc.). **B,** Multilayered doughnut chart summarizing the major tumor and molecular data details of the 353 PDX models described in this study. **C,** Number of PDX models established for each pediatric tumor entity. **D,** Pie charts highlighting the main clinical features of the ITCC-P4 PDX cohort, including tumor disease status and tumor site; main cancer categories; patient age at first diagnosis; and patient sex. Met, metastasis; Pri, primary; RR, refractory/relapse; U, unknown. **E,** Representation of the number of PDX models belonging to the main tumor molecular subgroups, annotated according to their epigenetic-based classification, for medulloblastoma (MB), ependymoma (EPN), HGG, and rhabdoid tumors. **F,** Number of neuroblastoma (NB), RS, and Ewing sarcoma (ES) PDX models presenting key/typical molecular alterations (*MYCN* amplification in neuroblastoma; molecular subtypes and FOXO*1* fusion status in rhabdomyosarcoma; EWSR*1* fusion status in Ewing sarcoma, respectively). HB, hepatoblastoma; MEL, melanoma; NHL, non–Hodgkin lymphoma; OS, osteosarcoma; RB, retinoblastoma; RT, extracranial malignant rhabdoid tumor; WT, Wilms tumor. **A,** Created in BioRender. Federico, A. (2026) https://BioRender.com/t07wpsv.

Downloaded from aacrjournals.org/cancerres/article-pdf/86/19/4755/3830682/can-25-5295.pdf by DKFZ - German Cancer Research Center user on 17 November 2026

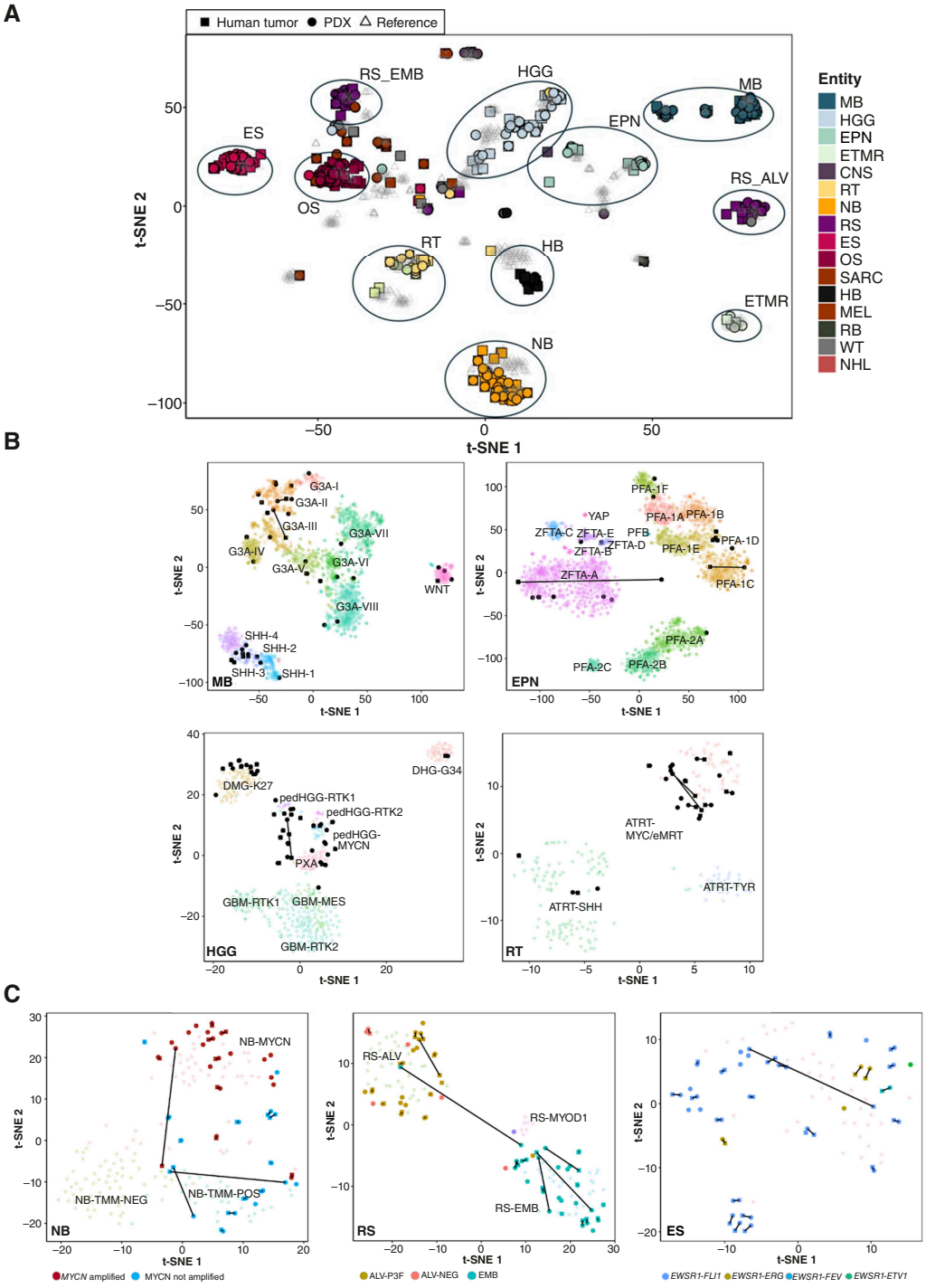


Figure 2.

DNA methylome and transcriptome of PDX models and matching patient tumors. **A,** t-distributed stochastic neighbor embedding (t-SNE) plot showing clustering analyses of ITCC-P4 methylation samples (PDXs: circles; patient tumors: squares), along with external tumor references covering a broad range of pediatric tumor entities. Clusters representing the common pediatric solid malignancies are highlighted. **B,** t-SNE panels showing subclustering analyses of ITCC-P4 methylation data grouped with consensus references for the main pediatric brain/CNS [medulloblastoma (MB), ependymoma (EPN), HGG] and rhabdoid tumor entities with relative molecular subtypes. Connecting lines are used to link PDX models (black dots) with their matching human tumor (black squares) data. **C,** Subclustering analyses of neuroblastoma (NB; left), RS (middle), and Ewing sarcoma (ES; right) methylation datasets, including ITCC-P4 and reference samples. Matching PDX and tumor data are connected. Key molecular status, such as *MYCN* amplification and detected *EWSR1* fusion events, are highlighted in the respective plots. HB, hepatoblastoma; MEL, melanoma; NHL, non–Hodgkin lymphoma; OS, osteosarcoma; RB, retinoblastoma; RT, extracranial malignant rhabdoid tumor; WT, Wilms tumor.

Downloaded from aacrjournals.org/cancerres/article-pdf/86/19/4755/3830682/can-25-5295.pdf by DKFZ - German Cancer Research Center user on 17 November 2026

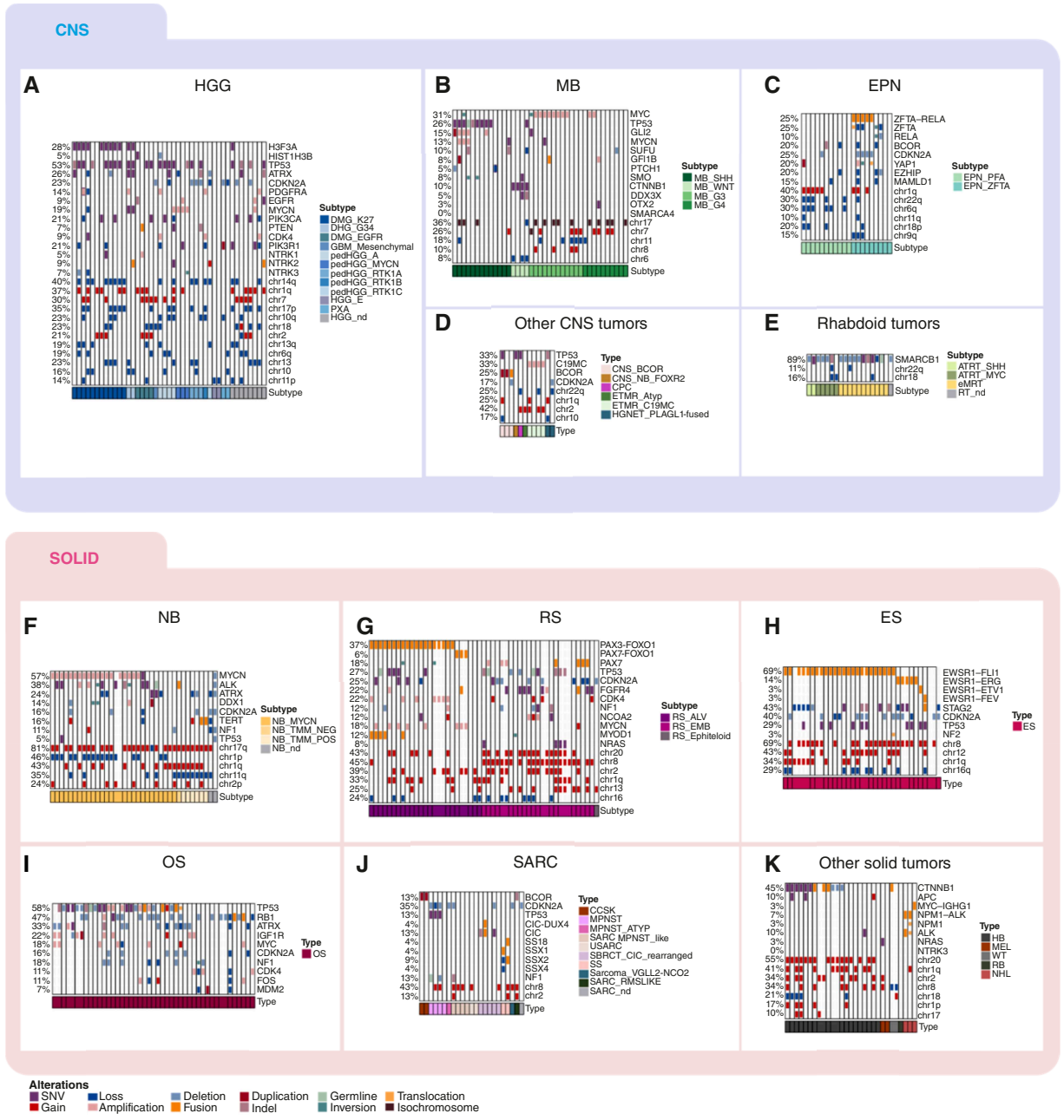


Figure 3.

OncoPrints depicting multiple genomic aberrations in the ITCC-P4 PDX cohort. OncoPrints report the mutational landscape of the PDX models established within the ITCC-P4 project. Each panel shows a comprehensive view of the key genetic alterations, including somatic and germline mutations (SNVs and indels), structural variants, and CNVs, for PDX models belonging to distinct tumor types: HGG (**A**), medulloblastoma (MB; **B**), ependymoma (EPN; **C**), other CNS tumors (**D**), rhabdoid tumors (**E**), neuroblastoma (NB; **F**), RS (**G**), Ewing sarcoma (ES; **H**), osteosarcoma (OS; **I**), SARC (**J**), and other solid tumors (**K**). For CNVs, *gain* and *loss* denote broad copy-number alterations, including chromosome- or chromosome-arm-level events as well as less extensive non-focal events encompassing specific genes; *amplification* and *deletion* denote focal copy-number events targeting specific gene(s). Tumor subtypes for each PDX model, if known and defined based on the methylation analyses, are reported. HB, hepatoblastoma; MEL, melanoma; NHL, non–Hodgkin lymphoma; RB, retinoblastoma; RT, extracranial malignant rhabdoid tumor; WT, Wilms tumor.

disease states and from primary (214; 61%) or metastatic (98; 28%) sites. For 41 models (11%), this information was not available. The collection covers CNS (121; 34%) and non-CNS tumors (232; 66%), including medulloblastoma (39), high-grade glioma (HGG; 43), ependymoma (20), embryonal tumor with multilayered rosettes (ETMR; 5), atypical teratoid rhabdoid tumor (ATRT; 7), and rare CNS types, as well as neuroblastoma (37), sarcoma [134; comprising osteosarcoma (45), rhabdomyosarcoma (RS; 51), Ewing sarcoma (35), and

Downloaded from aacrjournals.org/cancerres/article-pdf/86/19/4755/3830682/can-25-5295.pdf by DKFZ - German Cancer Research Center user on 17 November 2026

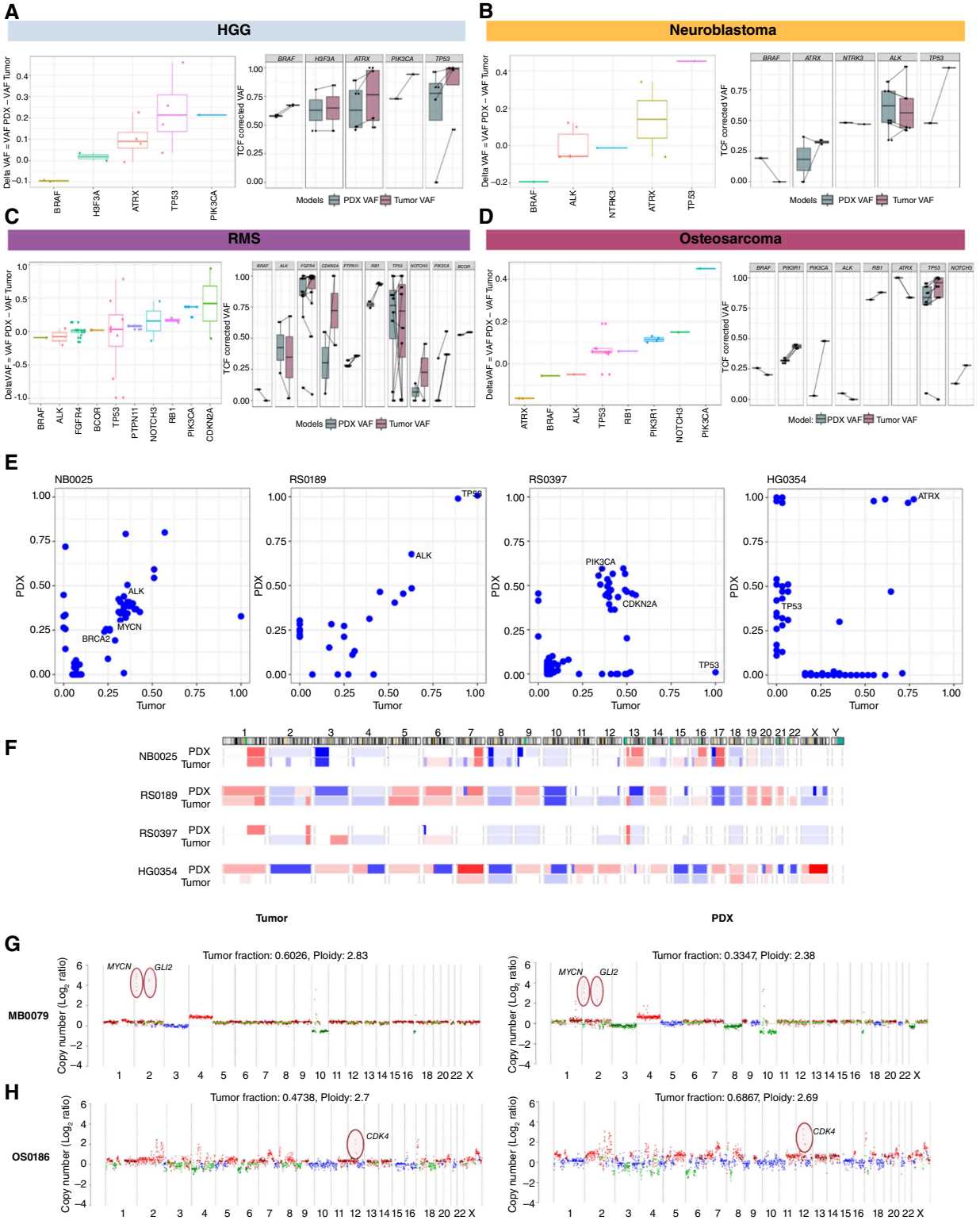


Figure 4.

Comparison of molecular alterations between patient tumors and matched PDXs. **A,** Left, DeltaVAF scores (on the *y*-axis; calculated by subtracting the TCF corrected VAF of the matching patient tumor from the TCF-corrected VAF of the PDX model) calculated for key driver genes (*BRAF*, *H3F3A*, *ATRX*, *PIK3CA*, *TP53*) in HGG tumors and PDXs. Positive deltaVAF scores indicate a higher frequency of the given mutation in the PDXs compared with their matched human tumors, whereas negative values define a higher mutation frequency in the original tumor. Highly concordant PDX–tumor (*Continued on the following page.*)

Downloaded from aacrjournals.org/cancerres/article-pdf/86/19/4755/3830682/can-25-5295.pdf by DKFZ - German Cancer Research Center user on 17 November 2026

rare subtypes (SARC; 23)], and 41 models representing other solid pediatric malignancies (**Fig. 1B–D**). The cohort covers the most common molecular subtypes and key driver genes seen in pediatric solid cancers (**Fig. 1E** and **F**; Supplementary Table S1).

Tumor molecular subtyping by DNA methylation analysis

PDX models were categorized using DNA methylation profiling followed by assessment in the Heidelberg CNS tumor and sarcoma classifiers (medRxiv 2025.06.30.25330543; 7), confidently classifying 239 out of 333 (72%) models (Supplementary Table S2). To validate this and classify the remaining models, we performed t-distributed stochastic neighbor embedding clustering of all methylation profiles alongside reference datasets ($n = 1{,}169$ cases; refs. 4, 5, 32–36). Most PDX models (333/353; 94%) clustered with reference samples reflecting the patients' diagnosis; 13 out of 333 (4%) were outliers. For outliers and PDX models without methylation data, classification was based on the original institutional pathologic and molecular diagnosis provided by the center that established the model, in combination with tumor type–specific oncogenic drivers identified by sequencing. Most primary patient tumors closely overlapped with corresponding PDX within entity-specific clusters (**Fig. 2A**). A Manhattan distance-based similarity index also confirmed high epigenetic concordance between PDX–tumor pairs (157/184 with distance <0.1; Supplementary Fig. S2A). Only models with unusual molecular features or a marked difference in tumor cell purity between patient and PDX samples (Supplementary Table S2) showed divergent clustering behavior.

Subclustering of CNS tumors revealed epigenetic profiles characteristic of major molecular subtypes, particularly in the heterogeneous brain tumors medulloblastoma (WNT, SHH, G3, G4), ependymoma (including the aggressive PFA and ZFTA-fusion subtypes), HGG (DMG_H3K27, DHG_G34, pedHGG_RTK1, pedHGG_MYCN, PXA), and rhabdoid tumors (MYC and SHH models; **Fig. 2B**; ref. 37). Neuroblastoma models separated by *MYCN* amplification status, and RS models showed clear alveolar/embryonal separation. Ewing sarcoma models clustered together although they displayed relatively broad interpatient heterogeneity, in line with previous reports (**Fig. 2C**; ref. 38).

Transcriptomic analysis of tumors and PDX models

Gene-based (top 1,000 most variable genes across the cohort) hierarchical clustering of PDX transcriptome data also showed aggregation by tumor type; in particular, coclustering of PDX models was driven by the expression of key pediatric cancer genes, such as *MYCN* and *ALK* (upregulated in neuroblastoma) or *MYOD1* (expressed in RS; Supplementary Fig. S2B). A comparison of patient and PDX tumor samples, based on differentially expressed genes, revealed a consistent preservation of the tumor-core signature from the original human tumors to the PDX models. However, compared with patient tumors, PDX models were commonly characterized by upregulation of cell cycle and DNA repair pathways and downregulation of immune and stromal gene signatures (Supplementary Table S3). These results corresponded to predicted tumor purity scores calculated on PDX and tumor samples based on omics data (Supplementary Tables S2 and S5), in line with previous reports (15, 17, 39).

The mutational landscape of the ITCC-P4 PDX models

Next, we investigated the mutational landscape of the PDX models, in combination with the available matching human tumors, by performing comprehensive genomic analysis (**Fig. 3**; Supplementary Fig. S3; Supplementary Table S4). Assessment of human-assigned reads in PDX-derived DNA sequencing libraries (Supplementary Fig. S4A) confirmed high human-read fractions in the large majority (97.6%) of models, whereas a few outliers ($n = 8$) with very low human-read fractions (<30%) also tended to show poor sequencing quality metrics, suggesting that these cases were influenced at least in part by technical library quality. Our analysis included calling of somatic SNVs, small indels, structural variations, gene fusions, and CNVs (Supplementary Fig. S4B). Germline mutation calling was performed whenever matched germline material was available (195/353; 55%). The full repertoire of genome-wide human tumor and PDX samples is provided at https://r2platform.com/itcc-p4.

We calculated the total number of somatic mutations detected by WES in paired PDX and tumor samples to define the TMB. We observed a higher TMB in PDX models compared with matching tumor cases (paired Wilcoxon test, P value = 0.00023; Supplementary Fig. S4C), with a greater difference seen between PDX and tumor cases of diagnostic samples ($P = 0.0028$; Supplementary Fig. S4D). Primary PDX tumor samples showed an overall higher TMB versus matching patient cases compared with metastatic ones (Supplementary Fig. S4E). Notably, observing the TMB scores for the mostly represented cancer entities with >1 PDX–tumor paired data available (HGG, ependymoma, medulloblastoma, ATRT/RT, neuroblastoma, RS, Ewing sarcoma, osteosarcoma, SARC, hepatoblastoma, Wilms tumor), neuroblastoma and osteosarcoma demonstrated a significantly pronounced disparity in TMB between the tumor and paired PDX, with the latter showing a higher TMB (Supplementary Fig. S4F).

CNS tumors and ATRT/extracranial rhabdoid tumor PDX models

HGG PDX models, mostly (30/43) established from primary disease, harbored the expected subtype-defining alterations, with *TP53* (23/43), *H3F3A* (12/43), *ATRX* (11/43), *CDKN2A* (10/43), and *MYCN* (8/43) being the most frequently mutated genes. Some other recurrent mutations in *BRAF*, *NRAS*, *PIK3CA*, and *NTRK1/2/3* alterations were also identified (**Fig. 3A**). Medulloblastoma models, again mostly (30/39) from primary disease and spanning all four molecular groups, showed subgroup-specific aberrations, including *MYC* amplifications in G3 (8/12) and *TP53* mutations in SHH

(*Continued.*) pairs show deltaVAF scores close to zero. Right, TCF-corrected tumor and PDX VAFs (*y*-axis) associated with the somatic SNVs affecting the most frequently mutated driver genes in HGG. Black lines connect matching pairs. **B,** DeltaVAF (left) and TCF-corrected VAF (right) plots showing the comparison of the mutation frequencies for key mutated drivers (*BRAF*, *ALK*, *NTRK3*, *ATRX*, *TP53*) in neuroblastoma PDX and tumor samples. **C,** DeltaVAF (left) and TCF-corrected VAF (right) plots showing the comparison of the mutation frequencies for key mutated drivers (*BRAF*, *ALK*, *FGFR4*, *BCOR*, *TP53*, *PTPN11*, *NOTCH3*, *RB1*, *PIK3CA*, *CDKN2A*) in RS PDX and tumor samples. **D,** DeltaVAF (left) and TCF corrected VAF (right) plots showing the comparison of the mutation frequencies for key mutated drivers (*ATRX*, *BRAF*, *ALK*, *TP53*, *RB1*, *PIK3R1*, *NOTCH3*, *PIK3CA*) in osteosarcoma PDX and tumor samples. **E,** Scatter plots showing the VAFs of somatic SNVs shared between the PDX models NB0025, RS0189, RS0397, HG0354, and their respective patient tumors. Key mutated genes are highlighted. **F,** Heatmap of the whole-genome CNV landscape observed in the PDX models NB0025, RS0189, RS0397, HG0354, and their respective patient tumors. Gains of chromosome regions are shown in red, whereas blue segments represent region losses. **G,** Genome-wide plots (generated by ichorCNA) showing the copy-number ratio ($\log_2$) and focal amplification events of *MYC* and *GLI2* in the MB0079 PDX model (right) and tumor (left). Tumor fraction and ploidy are reported for both samples. **H,** Genome CNV plots of OS0186 PDX (right) and matching tumor (left). *CKD4* amplification (red circled areas) is observed in both conditions.

Downloaded from aacrjournals.org/cancerres/article-pdf/86/19/4755/3830682/can-25-5295.pdf by DKFZ - German Cancer Research Center user on 17 November 2026

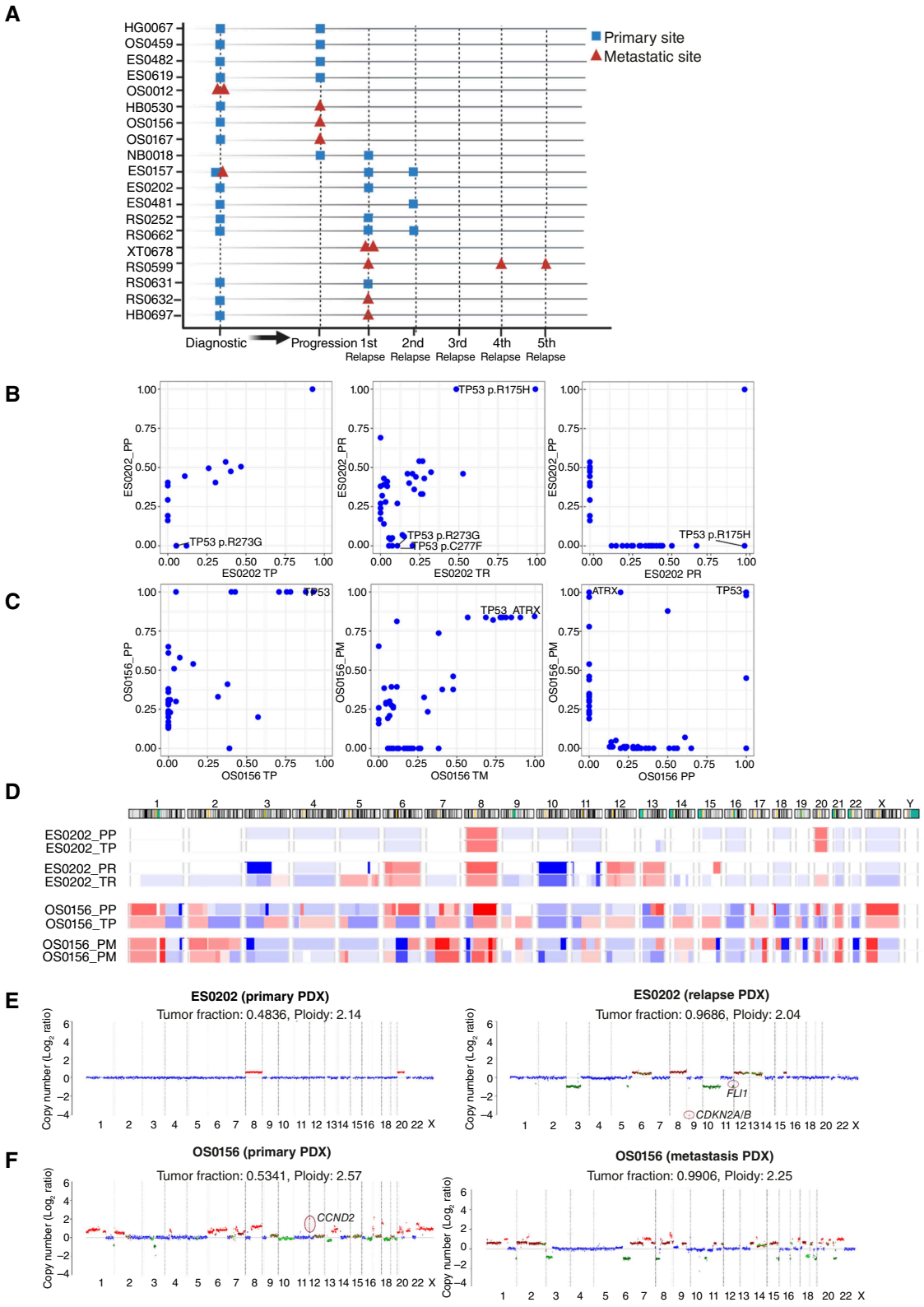


Figure 5.

Comparative analysis of the "serial" PDX models reveals tumor event–specific molecular characteristics. **A,** Schematic overview of the subset ($n = 40$) of serial PDX models established from multiple patient tumor events over the course of the disease. The tumor site from which (*Continued on the following page.*)

Downloaded from aacrjournals.org/cancerres/article-pdf/86/19/4755/3830682/can-25-5295.pdf by DKFZ - German Cancer Research Center user on 17 November 2026

models (9/13). Other SHH-specific gene variants included *GLI2* (4/13) and *MYCN* (3/13) amplifications (**Fig. 3B**). Ependymoma models with 17/20 from relapsed/refractory disease represented only the two most aggressive subtypes: PFA and ZFTA fusion; high-risk CNV features, including 1q gain (8/20) and 6q loss (6/11 PFA), were prevalent (**Fig. 3C**). Other rare CNS tumor types included in our cohort were ETMR (4/5 models presenting the typical *C19MC* amplification), BCOR-altered tumors ($n = 3$), HGNET *PLAG1*-fused tumors ($n = 2$), CNS neuroblastoma ($n = 1$), and choroid plexus carcinoma, $n = 1$; **Fig. 3D**). ATRT ($n = 7$) and extracranial rhabdoid tumor models ($n = 12$), mostly from primary disease (17/19), carried the expected defining alterations in SMARCB1 in 17 out of 19 cases (SNVs $n = 4/19$; indels $n = 2/19$; copy loss $n = 11/19$; undetected in 2/19; **Fig. 3E**).

Neuroblastoma PDX models

Among the 37 neuroblastoma models, including 10 from diagnostic primary tumors, *MYCN* alterations were present in 21 out of 37 (predominantly focal amplification, 19/21). Additional driver mutations or alterations included *ALK* (14/37), *ATRX* (9/37), *CDKN2A* (6/37), and *DDX1* (5/37). The most frequent CNVs were chr17q gain (30/37) and 1p loss (17/37); CNVs associated with poor outcomes (40, 41), such as 1p loss (17/37), 1q gain (16/37), and 11q loss (13/37), were also observed (**Fig. 3F**).

Soft-tissue sarcoma/bone sarcoma PDX models

RS PDX models ($n = 51$), including 14 from diagnostic primary tumors, showed a clear alveolar/embryonal distinction: alveolar RS models were defined by *PAX3::FOXO1* (19/25) or *PAX7::FOXO1* (3/25) fusions and *CDK4* amplification/gain (11/25), whereas embryonal RS models showed frequent *TP53* (9/25), *BCOR* (8/25), *FGFR4* (9/25), *CDKN2A* (8/25), *NRAS* (4/25), and *NF1* (4/25) alterations (**Fig. 3G**). One model was annotated as epithelioid based on pathologic findings and presented a distinct molecular status. Ewing sarcoma models ($n = 35$), including 13 from diagnostic primary tumors, were defined by *EWSR1::FLI1* fusion (28/35) or other *EWSR1::ETS* fusions (7/35); recurrent mutations conferring adverse outcomes (42) in *STAG2* (15/35) and *TP53* (10/35), co-occurring in five models, and *CDKN2A* loss (14/35) were also prominent (**Fig. 3H**). Osteosarcoma models ($n = 45$), including 13 from diagnostic primary tumors, reflected their known genomic complexity (Supplementary Fig. S4), with frequent *TP53* (26/45), *RB1* (21/45), and *ATRX* (12/45) alterations (**Fig. 3I**). PDX models representing other rare sarcoma subtypes ($n = 23$), including malignant peripheral nerve sheath tumors, clear-cell sarcoma of the kidney, synovial sarcoma, CIC-rearranged soft-tissue round cell sarcoma (SBRCT_CIC_rearranged), and undifferentiated sarcoma, displayed entity-defining events such as *SS18*::SSX fusions in synovial sarcoma and *CIC::DUX4* fusions in *CIC*-rearranged tumors (**Fig. 3J**).

Other PDX models

The remaining models include hepatoblastoma (21), defined by recurrent *CTNNB1* mutations (12/21); two pediatric melanoma models; two Wilms tumor models; and three non–Hodgkin lymphoma models with *ALK* or *MYC* fusions (**Fig. 3K**).

Assessing PDX model fidelity compared with matching patient tumors

We compared molecular data from 124 matched human tumor/PDX pairs (Supplementary Fig. S3; Supplementary Table S4). Most PDX models with paired tumor WES data (96/124; 77%) showed maximal tumor cell fraction scores, confirming enriched tumor purity relative to patient samples (Supplementary Fig. S5A; Supplementary Table S5). Following correction of VAFs for tumor cell content, 65% of pairs (81/124) showed moderate-to-high concordance (Pearson $r > 0.4$; median $r = 0.59$) for shared somatic variants (Supplementary Table S5).

Focusing on key driver genes (*ALK*, *ATRX*, *BRAF*, *BCOR*, *CDKN2A*, *FGFR4*, *H3F3A*, *NTRK3*, *NOTCH3*, *PIK3CA*, *PTPN11*, *RB1*, *TP53*; 103/124 pairs presented a mutation for one or more of these genes), 74% of shared mutations (76/103 comparisons) showed stable VAFs between tumor and PDX (deltaVAF −0.2 to +0.2; **Fig. 4A–D**; Supplementary Fig. S5B). Notable exceptions included HGG models with enriched *TP53*, *PIK3CA*, and *ATRX* mutations in PDX, whereas *BRAF* mutations were selectively absent in PDX, suggesting subclonal selection upon engraftment (**Fig. 4A–E**). Neuroblastoma and RS models showed overall strong VAF concordance with their tumors (**Fig. 4B**, **C**, and **E**), with few exceptions like the RS0397 model, in which a *TP53* mutation was exclusively seen in the tumor data (**Fig. 4E**); similarly, osteosarcoma models frequently exhibited enrichment of *TP53* and *RB1* SNVs in PDX (**Fig. 4D** and **E**). CNV profiles were similarly concordant in most pairs (**Fig. 4E–H**; Supplementary Fig. S5C and S5D) though a subset of models (e.g., RS0397, HG0354) showed divergent CNV landscapes. These discrepancies likely reflect differences in tumor purity, immune microenvironment, and subclonal selection during xenograft establishment.

Overall, the PDXs included in this study exhibited good molecular concordance with their respective human tumors in terms of VAFs and preservation of the overall clonal identity, whereas weaker correlations were observed in a subset of pairs, as well as sporadic mutually exclusive gene alterations.

Serial PDX models: modeling tumor progression

Serial PDX models were established from 40 tumors from 19 patients, spanning diagnostic/posttreatment, primary/relapse, and metastasis-derived pairs (**Figs. 3** and **5A**; Supplementary Figs. S3 and S6). These models captured key molecular events in tumor progression: for example, in patient ES0202 with Ewing sarcoma, a *TP53* R175H mutation was acquired exclusively in relapse-derived samples, consistent with treatment-driven selection (**Fig. 5B**). In patient OS0156 with osteosarcoma, an *ATRX* mutation was detectable only in the metastasis-derived sample and PDX (**Fig. 5C**). Serial models frequently revealed the emergence of new CNVs at later disease stages, including *CDKN2A/B* deletion and *FLI1* loss in the relapsed ES0202 model, whereas *CCND2* gain, shown in the

(*Continued*.) multiple PDX were generated is highlighted. **B,** VAF plots showing the correlation of mutation frequencies for the following combinations of the Ewing sarcoma models ES0202: patient primary tumor (PT) vs. primary PDX (PP; left); patient relapse original tumor (TR) vs. relapse PDX (PR; middle); and primary PDX vs. relapse PDX (right). TP53 gene mutations are highlighted. **C,** VAF plots showing the correlation of mutation frequencies for the following combinations of the osteosarcoma models OS0156: patient primary tumor (PT) vs. primary PDX (PP; left); patient metastatic tumor (TM) vs. metastatic PDX (PM; center); primary PDX (PP) vs. metastatic PDX (PM; right). TP53 and ATRX gene mutations are highlighted. **D,** CNV heatmap showing chromosome gains and/or losses for PDX models ES0202 (primary and relapse), OS0156 (primary and metastasis), and related matched patient samples. **E,** CNV plots of ES0202 (primary and relapse) PDX models. Key focal events are highlighted in red circled areas. **F,** CNV plots of OS0156 (primary and metastasis) PDX models. Key focal events are highlighted in red circled areas. **A,** Created in BioRender. Federico, A. (2026) https://BioRender.com/4jq7600.

Downloaded from aacrjournals.org/cancerres/article-pdf/86/19/4755/3830682/can-25-5295.pdf by DKFZ - German Cancer Research Center user on 17 November 2026

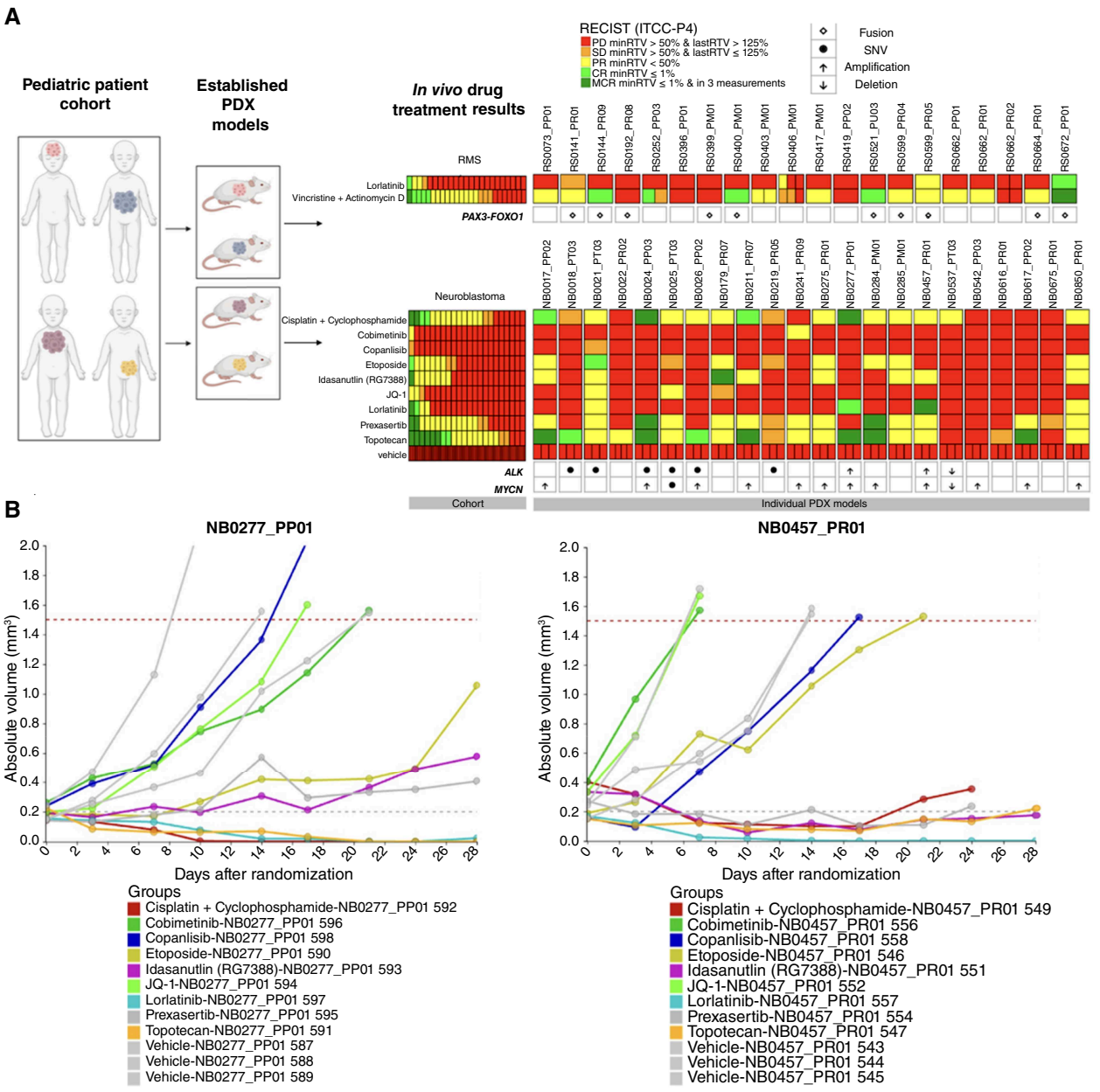


Figure 6.

In vivo drug response profiling in the ITCC-P4 PDX cohort. Neuroblastoma and RS PDX models from the ITCC-P4 cohort were treated in single-mouse *in vivo* studies with standard-of-care (SOC) regimens and additional experimental drugs and compared with control mice. Responses were monitored longitudinally and summarized in the heatmap (**A**) using RECIST-based criteria adapted for PDX models based on tumor volume. Each row represents a PDX model, and each column represents a treatment; the relevant mutational status of each model is indicated. Representative tumor growth curves (**B**) for two neuroblastoma models illustrate treatment responses over time. **A,** Created in BioRender. Federico, A. (2026) https://BioRender.com/y1xy9vx.

diagnostic OS0156, could not be detected in the matching metastasis-derived PDX model (**Fig. 5D–F**; Supplementary Table S4).

Calculation of the CCFs enabled inference of clonal architecture and evolutionary trajectories from somatic SNVs and copy-number analysis in a subset of serial PDX models. This clonal evolution analysis identified changes in clonal prevalence, with both contracting and expanding subclonal cellular populations across disease stages, highlighting dynamic tumor evolution. In OS0156 (diagnostic–metastatic) and ES0157 (diagnostic–metastatic–multiple relapses) sequential models, we observed dynamic shifts across the different disease stages of CCFs relative to somatic SNVs affecting selected genes, with a drastic reduction of POU6F2 gene CCF in the OS0156 metastatic PDX versus primary PDX (99.2% vs. 18.2%), and fluctuations of UBXN11 CCF from primary (87.3%), metastatic (39.2%), and relapse-derived (47.2% and 25.5%) models (Supplementary Fig. S7).

Downloaded from aacrjournals.org/cancerres/article-pdf/86/19/4755/3830682/can-25-5295.pdf by DKFZ - German Cancer Research Center user on 17 November 2026

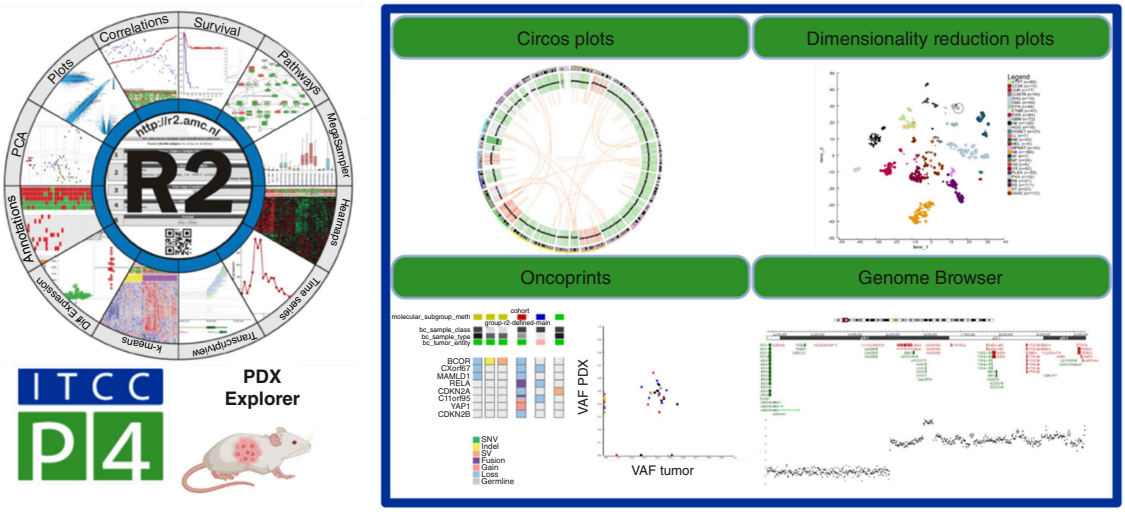


Figure 7.

R2 platform–ITCC-P4 PDX datascope. A full report of the clinical information, PDX growth details, and molecular characterization for each ITCC-P4 PDX model is available on the ITCC-P4 Datascope in R2 (r2-itccp4. amc.nl). Here, several features were implemented to integrate multiomics data and to help users in the investigation and visualization of the molecular readouts, such as interactive plots (circos, t-SNE, heatmap, etc.), curated OncoPrints, and the R2 embedded genome browser. Created in BioRender. Federico, A. (2026) https://BioRender.com/dm5soee.

Altogether, serial models revealed a persistence of driver events across the disease course, with a frequent emergence of new driver alterations such as *TP53* upon relapse. However, clonal evolution analysis revealed a shift in clonal prevalence between PDX models established from primary and metastatic samples and from diagnosis and relapse, including both contracting and expanding cellular populations.

In vivo drug sensitivity: implications for targeted therapies

As proof of concept, we evaluated standard-of-care drugs and the ALK inhibitor lorlatinib in 22 neuroblastoma and 20 RS models. In neuroblastoma, topotecan sensitivity was enriched in *MYCN*-amplified models (7/8 responders), consistent with increased replication stress in this subtype, whereas etoposide showed greater efficacy in *MYCN*–nonamplified models. Lorlatinib was highly effective in two models (NB0457_PR and NB0277_PR) with *ALK* amplification and elevated *ALK* expression, confirming *ALK* amplification as a predictive biomarker for lorlatinib sensitivity in neuroblastoma (43); notably, five models with hotspot *ALK* point mutations (F1174L, R1275Q) were not sensitive to lorlatinib (**Fig. 6**).

In RS, vincristine/actinomycin D treatment yielded high sensitivity in 5 out of 20 models and partial responses in 9 out of 20; among the 14 responsive models, eight (57%) harbored *PAX3/7::FOXO1* fusions. Lorlatinib showed high efficacy in two models harboring *ALK* fusions (RS0599_PR05 and RS0141_PR01), supporting *ALK* fusions as a biomarker for lorlatinib response also in RS (**Fig. 6**). These results underscore the value of correlating *in vivo* drug response with comprehensive molecular characterization.

The ITCC-P4 data portal

Molecular characterization data of WHO-implicated genes from the ITCC-P4 cohort are accessible to the global scientific community via the R2 ITCC-P4 PDX data scope portal (https://r2platform.com/itcc-p4/). Upon confirmation, noncommercial usage data on all molecular alterations are released. Researchers can select models by entity, oncogenic driver, or biomarker for proof-of-concept *in vivo* studies. The portal covers the full multiomics dataset described here and additional generated models, enhancing translational potential and accelerating the discovery of novel therapeutic targets (**Fig. 7**).

Discussion

Significant progress has been made in understanding the molecular basis of pediatric tumors, yet valid and predictive preclinical models for high-risk childhood cancers remain urgently needed. PDX models stand out for their stability across passages, comprehensive molecular profiling capacity, and close recapitulation of the genomic, epigenetic, and transcriptomic landscape of original human tumors. For all these reasons, PDX models have already strongly contributed to preclinical testing (medRxiv 2025.08.10.25333051; ref. 44). However, the use of PDX models in preclinical research also faces constraints, both technical (such as engraftment success rates, immunodeficiency of host mice, and the time-consuming, costly process for model establishment) and biological (including limited availability of certain tumor types and genomic evolution). The ITCC-P4 platform directly addresses this need with a large, heterogeneous, and molecularly well-characterized PDX collection.

Our PDX repertoire is an excellent representation of distinct pediatric tumor types, subtypes, and molecular vulnerabilities. We observed enrichment of aggressive molecular phenotypes, including chr1q gain, *CDKN2A/B* loss, *MYC* amplification, and *STAG2*, *TP53*, and *ATRX* mutations (45). Rarer and less aggressive tumor families remain underrepresented, reflecting the established challenge that low-grade tumors engraft poorly. The ITCC-P4 cohort will be expanded to include leukemia and lymphoma models, aiming for complete coverage of all known high-risk pediatric cancer subtypes.

A key strength of this study is the first large-scale integration of PDX molecular characterization with matching patient tumor and

Downloaded from aacrjournals.org/cancerres/article-pdf/86/19/4755/3830682/can-25-5295.pdf by DKFZ - German Cancer Research Center user on 17 November 2026

germline data across diverse pediatric cancer types. The multiomics approach—combining DNA methylome profiling, WES, lcWGS, and RNA-seq—was particularly powerful for defining oncogenic drivers in cases in which single-omics analyses were insufficient. DNA methylation profiling was especially valuable for molecular subtype classification and enabled direct epigenomic comparison between patient tumors and PDXs.

As the platform expands with the integration of novel PDXs, as well as GEMMs and organoid models, coupled with advancements in next-generation sequencing tools and analyses, incorporating additional techniques such as chromatin immunoprecipitation sequencing, Assay for Transposase-Accessible Chromatin using sequencing, and DNA and RNA single-cell sequencing becomes imperative for obtaining a thorough overview of PDX models. These methods play crucial roles in exploring gene regulation and understanding epigenetic modifications and/or cellular diversity between tumor–PDX pairs. Beyond methylation profiling, exploration of the PDX models, and whenever possible, the matched tumor, with regard to histone modifications, chromatin accessibility, and nucleosome occupancy, as well as genome organization and long-range genome interactions, will be explored in bulk and at a single-cell level. This will enable the identification of rare cell types and elucidate dynamic changes in gene expression during development and disease progression or in response to treatments in PDX models.

The molecular comparison between human tumors and matched PDXs demonstrated high concordance for genetic variants, TMB, and epigenomic/transcriptomic profiles in the majority of pairs. Observed discrepancies in VAF enrichment likely reflect differences in tumor cellularity, loss of the immune microenvironment during engraftment (46), and subclonal selection. These findings reinforce the importance of tumor purity correction when interpreting PDX–tumor comparisons and highlight that a minority of PDX models may represent a distinct subclone of the original tumor.

Serial PDX models representing different disease stages from the same patients provide a powerful resource for studying tumor evolution, treatment resistance mechanisms, and the emergence of new driver alterations upon relapse. Our findings demonstrate the persistence of founding driver events across the disease course, with frequent acquisition of TP53 mutations at relapse and dynamic shifts in clonal architecture between primary and metastatic or relapsed disease.

The proof-of-concept drug testing data align closely with the molecular profiles of the models, validating the platform's utility for biomarker-driven preclinical studies. The identification of ALK amplification—but not point mutations—as a predictor of lorlatinib sensitivity in neuroblastoma, and ALK fusions in RS, illustrates how the platform can directly inform stratified treatment strategies.

The ITCC-P4 platform is operated as a nonprofit entity (ITCC-P4 gGmbH; https://itccp4.com/: ITCC-P4 GmbH Paediatric Preclinical Proof of Concept Platform) in collaboration with three CROs. PDX models are not sold but are accessible for preclinical drug testing by academic and industrial users via standardized, ethically compliant workflows adhering to the 3Rs principle. All models remain available for scientific collaboration through the academic consortium partners, and the full molecular dataset is openly accessible via the R2 data portal. The possibility of choosing between different models depending on tumor type and subtype, and molecular features, as well as the fully established workflow within the ITCC-P4 gGmbH, are of interest to the scientific community.

In conclusion, the ITCC-P4 platform represents a powerful and sustainable resource for investigating pediatric cancer biology and accelerating the development of innovative therapeutic options for children with cancer.

Data Availability

The curated multiomics data are accessible via the R2 ITCC-P4 PDX Datascope portal (http://r2platform.com/itcc-p4/). Raw sequencing data are accessible via the European Genome-phenome Archive, access number: EGAS00001008330). Any other data shown in this study are available upon request. For inquiries about the data, please contact ITCC-P4 gGmbH (info@itccp4.com).

Authors' Disclosures

J.J. Waterfall reports personal fees and other support from Mnemo Therapeutics and personal fees from Egle Therapeutics outside the submitted work. J.A. Wierzbinska reports other support from Bayer AG during the conduct of the study, as well as other support from Bayer AG outside the submitted work. A. Schlicker reports other support from Bayer AG during the conduct of the study, as well as other support from Bayer AG outside the submitted work. S. Brabetz reports personal fees from Champions Oncology, Inc. outside the submitted work. A.-L. Böttcher reports grants from the Innovative Health Initiative Joint Undertaking during the conduct of the study. D.T.W. Jones reports other support from Heidelberg Epignostix GmbH and personal fees from Day One Biopharmaceuticals and Ipsen Pharma outside the submitted work. O. Witt reports grants from Dietmar-Hopp-Stiftung (KiTZ CTU 2.0 Program) and Viessmann Stiftung (Pediatric Drug Development) during the conduct of the study, as well as personal fees from Ipsen and Novartis and grants from Day One Biopharmaceuticals and BVD outside the submitted work. T. Milde reports other support from Ipsen Pharma GmbH and grants from Biomed Valley Discoveries and Day One Biopharmaceuticals outside the submitted work. A. Eggert reports personal fees from Recordati and VANUDIS outside the submitted work. N. Huebener reports grants from Charité – Universitätsmedizin Berlin during the conduct of the study. J.-H. Klusmann reports personal fees from Pfizer and Boehringer Ingelheim outside the submitted work. K.-M. Debatin reports grants from the German Research Council during the conduct of the study. S. Bomken reports grants from Cancer Research UK, JGW Patterson Foundation, Children's Cancer North, Medical Research Council, Kay Kendall Leukaemia Fund, and European Research Council during the conduct of the study. C.D. Guttke reports other support from Johnson and Johnson Innovative Medicine outside the submitted work. P. Hamerlik reports other support from AstraZeneca during the conduct of the study. M.M. Hattersley reports other support from AstraZeneca outside the submitted work, as well as employment with AstraZeneca. M. Zapotocky reports personal fees and nonfinancial support from AstraZeneca, personal fees from Merck, and nonfinancial support from Ipsen outside the submitted work. J. Gojo reports grants, personal fees, and nonfinancial support from Roche; personal fees from Norgine, Medical University International, Ipsen, and Novartis; and grants and personal fees from Rhythm Pharmaceuticals outside the submitted work. K. Scotlandi reports grants from the European Union during the conduct of the study. M.C. Manara reports grants from European Union during the conduct of the study. L. Landuzzi reports grants from the European Union during the conduct of the study. J. Hoffmann reports other support from Experimental Pharmacology and Oncology Berlin-Buch during the conduct of the study. D.J. Shields reports other support from Pfizer Inc. during the conduct of the study. H.N. Caron reports employment with Hoffmann-La Roche and ownership of Hoffmann-La Roche stocks. S.M. Pfister reports grants from IMI-2 Funding involving Roche, Bayer, AstraZeneca, Pfizer, Eli Lilly, Janssen, PharmaMar, Amgen, and Servier during the conduct of the study, as well as other support from Heidelberg Epignostix outside the submitted work. M. Kool reports grants from the Innovative Medicines Initiative 2 and other support from Bayer, Roche, Servier, Pfizer, and Amgen during the conduct of the study. G. Schleiermacher reports grants from Roche, Pfizer, Amgen, Imagine for Margo, Annenberg Foundation, Association Hubert Gouin Enfance et Cancer, Fédération Enfants Cancers Santé, Bagouz à Manon, Les amis de Claire, INCA, Agence Nationale de la Recherche, Fondation ARC pour la Recherche contre le Cancer, and Ligue contre le Cancer during the conduct of the study, as well as grants from MSD Avenir, Bristol Myers Squibb, and Servier and other support from Recordati/EUSA Pharma outside the submitted work. No disclosures were reported by the other authors.

Downloaded from aacrjournals.org/cancerres/article-pdf/86/19/4755/3830682/can-25-5295.pdf by DKFZ - German Cancer Research Center user on 17 November 2026

Authors' Contributions

A. Federico: Conceptualization, resources, data curation, software, formal analysis, supervision, funding acquisition, validation, investigation, visualization, methodology, writing–original draft, project administration, writing–review and editing. **A. Gopisetty:** Conceptualization, resources, data curation, software, formal analysis, supervision, funding acquisition, validation, investigation, visualization, methodology, writing–original draft, project administration, writing–review and editing. **D. Surdez:** Conceptualization, resources, data curation, software, formal analysis, supervision, funding acquisition, validation, investigation, visualization, methodology, writing–original draft, project administration, writing–review and editing. **Y. Iddir:** Resources, data curation, software, formal analysis, investigation, methodology, writing–review and editing. **R.J. Autry:** Resources, data curation, formal analysis, validation, investigation, methodology, writing–review and editing. **J.J. Waterfall:** Resources, data curation, formal analysis, supervision, validation, investigation, visualization, methodology, writing–original draft, writing–review and editing. **E. Saberi-Ansari:** Resources, data curation, software, formal analysis, writing–original draft, writing–review and editing. **C. Bobin:** Resources, formal analysis, investigation, methodology, writing–original draft. **S. Ballet:** Resources, investigation, methodology, writing–original draft. **G. Pierron:** Resources, formal analysis, investigation, methodology, writing–original draft. **J.A. Wierzbinska:** Resources, data curation, formal analysis, validation, investigation, writing–original draft. **A. Schlicker:** Resources, data curation, formal analysis, validation, investigation, methodology, writing–original draft. **M. Sill:** Resources, data curation, formal analysis, writing–original draft. **R. Volckmann:** Resources, data curation, software, writing–original draft. **D.A. Zwijnenburg:** Resources, data curation, software, writing–original draft. **A. Mackay:** Resources, data curation, software, writing–original draft. **S. Zaïdi:** Resources, formal analysis, writing–original draft. **A. Saint-Charles:** Resources, data curation, formal analysis, methodology, writing–original draft. **N. Mack:** Resources, data curation, formal analysis, writing–original draft. **B. Schwalm:** Resources, data curation, formal analysis, writing–original draft. **S. Brabetz:** Methodology. **L. Weiser:** Resources, data curation, software, formal analysis, writing–original draft. **I. Buchhalter:** Conceptualization, resources, data curation, software, formal analysis, validation, investigation, visualization, methodology, writing–original draft. **C. Previti:** Resources, data curation, software, formal analysis, investigation, visualization, methodology, writing–original draft. **A.-L. Böttcher:** Resources, data curation, methodology, project administration, writing–review and editing. **F. Iradier:** Conceptualization, resources, data curation, funding acquisition, writing–review and editing. **E.-M. Rief:** Resources, data curation, writing–original draft, project administration. **D.T.W. Jones:** Conceptualization, data curation, software, formal analysis, supervision, funding acquisition, validation, investigation, methodology, writing–original draft. **O. Witt:** Resources, data curation, investigation, writing–original draft. **F. Westermann:** Resources, data curation, software, formal analysis, supervision, validation, investigation, visualization, methodology, writing–original draft. **T. Milde:** Resources, data curation, writing–original draft. **A. Eggert:** Resources, data curation, writing–original draft. **N. Huebener:** Resources, data curation, writing–original draft. **J.H. Schulte:** Resources, data curation, writing–original draft. **S. Colombetti:** Resources, data curation, software, formal analysis, funding acquisition, writing–original draft. **L. Chesler:** Resources, data curation, software, formal analysis, writing–original draft. **E.R. Tucker:** Resources, data curation, investigation, methodology, writing–review and editing. **A. Morcavallo:** Resources, data curation, investigation, methodology, writing–review and editing. **F. Lorenzi:** Resources, data curation, validation, investigation, methodology, writing–review and editing. **H. Kovar:** Resources, data curation, formal analysis, visualization, methodology, writing–original draft. **J.-H. Klusmann:** Resources, data curation, formal analysis, writing–original draft. **K.-M. Debatin:** Resources, data curation, formal analysis, writing–original draft. **S. Bomken:** Resources, data curation, methodology, writing–original draft. **C.D. Guttke:** Resources, data curation, funding acquisition, writing–original draft. **P. Hamerlik:** Resources, data curation, funding acquisition, writing–original draft. **M.M. Hattersley:** Resources, data curation, funding acquisition, writing–original draft. **M. Garcia:** Resources, data curation, funding acquisition, writing–original draft. **F. Colland:** Resources, data curation, funding acquisition, writing–original draft. **A. Strougo:** Resources, data curation, funding acquisition, writing–original draft. **P. Aviles:** Resources, data curation, funding acquisition, writing–original draft. **M. Zapotocky:** Resources, data curation, methodology, writing–original draft. **D. Sumerauer:** Resources, data curation, methodology, writing–original draft. **J. Gojo:** Resources, data curation, software, formal analysis, visualization, methodology, writing–original draft. **W. Berger:** Resources, data curation, investigation, visualization, methodology, writing–original draft. **D. Lötsch-Gojo:** Resources, data curation, methodology, writing–original draft. **J. Schueler:** Conceptualization, resources, data curation, formal analysis, funding acquisition, writing–original draft. **E.J. Girard:** Resources, data curation, investigation, writing–original draft. **J.M. Olson:** Resources, data curation, formal analysis, writing–original draft. **B.W. Schäfer:** Resources, data curation, formal analysis, visualization, methodology, writing–original draft. **M. Wachtel:** Resources, data curation, investigation, visualization, methodology, writing–original draft. **J.J. Molenaar:** Resources, data curation, methodology, writing–original draft. **B. Dumevska:** Resources, data curation, methodology, writing–original draft. **E. Fernandez Potente:** Resources, data curation, writing–original draft. **C. Jones:** Resources, data curation, investigation, methodology, writing–original draft. **A.M. Carcaboso:** Resources, data curation, investigation, methodology, writing–original draft. **E. Indersie:** Resources, data curation, funding acquisition, writing–review and editing. **S. Cairo:** Resources, data curation, funding acquisition, writing–original draft. **K. Scotlandi:** Resources, data curation, formal analysis, methodology, writing–original draft. **M.C. Manara:** Resources, data curation, formal analysis, methodology, writing–original draft. **L. Landuzzi:** Resources, data curation, methodology, writing–original draft. **A. Di Giannatale:** Resources, data curation, formal analysis, methodology, writing–original draft. **P. Gasparini:** Resources, data curation, investigation, methodology, writing–original draft. **M. Moro:** Resources, data curation, methodology, writing–original draft. **D. Gürgen:** Resources, data curation, formal analysis, funding acquisition, writing–original draft. **J. Hoffmann:** Resources, data curation, funding acquisition, methodology, writing–original draft. **M.E. Marques da Costa:** Resources, data curation, investigation, methodology, writing–original draft. **B. Geoerger:** Resources, data curation, methodology, writing–original draft. **O. Delattre:** Resources, data curation, software, formal analysis, investigation, visualization, methodology, writing–original draft. **D.J. Shields:** Conceptualization, resources, data curation, software, formal analysis, funding acquisition, validation, investigation, visualization, methodology, writing–original draft, project administration. **H.N. Caron:** Conceptualization, resources, data curation, software, formal analysis, funding acquisition, investigation, visualization, methodology, writing–original draft, project administration. **G. Vassal:** Conceptualization, resources, funding acquisition, writing–original draft, project administration. **L.F. Stancato:** Conceptualization, resources, data curation, software, supervision, funding acquisition, methodology, writing–original draft, project administration, writing–review and editing. **S.M. Pfister:** Conceptualization, resources, data curation, software, formal analysis, supervision, funding acquisition, validation, investigation, visualization, methodology, writing–original draft, project administration, writing–review and editing. **N. Jäger:** Resources, data curation, investigation, visualization, methodology, writing–original draft, writing–review and editing. **J. Koster:** Conceptualization, resources, data curation, software, formal analysis, supervision, funding acquisition, validation, investigation, visualization, methodology, writing–original draft, project administration, writing–review and editing. **M. Kool:** Conceptualization, resources, data curation, software, formal analysis, supervision, funding acquisition, validation, investigation, visualization, methodology, writing–original draft, project administration, writing–review and editing. **G. Schleiermacher:** Conceptualization, resources, data curation, software, formal analysis, supervision, funding acquisition, validation, investigation, visualization, methodology, writing–original draft, project administration, writing–review and editing.

Acknowledgments

ITCC-P4 IMI-2 project: Funding sources/grant numbers: This project has received funding from the Innovative Medicines Initiative 2 Joint Undertaking under grant agreement number 116064. This joint undertaking receives support from the European Union's Horizon 2020 research and innovation program and EFPIA. The project was supported by funding from Bayer, Roche, and Servier within the IMI2 ITCC P4 program. Molecular characterization was supported by funding from Roche, Pfizer, and Amgen within the IMI2 ITCC P4 program. INFORM/German Cancer Research Center (DKFZ), Germany: The INFORM program is financially supported by the DKFZ, several German health insurance companies, the German Cancer Consortium (DKTK), the German Federal Ministry of Education and Research, the German Federal Ministry of Health, the Ministry of Science, Research and the Arts of the State of Baden-Württemberg, the German Cancer Aid, the German Childhood Cancer Foundation (DKS), RTL television, and the aid organization BILD hilft e.V. (Ein Herz für Kinder) and the generous private donation of the Scheu family. The authors would like to express their sincere thanks to Carsten Maus and Erjia Wang (Genomics and Proteomics Core Facility, DKFZ) and Gregor Warsow (Omics IT and Data Management Core Facility, DKFZ) for their highly dedicated support in data management and processing and to Gnanaprakash Balasubramanian and Rolf Kabbe (Division of Pediatric Neuro-oncology, DKFZ) for their sincere and dedicated contribution to the bioinformatics analyses. Institut Curie, France: Resources/Facilities: At Institut Curie, this work was supported by Imagine for

Downloaded from aacrjournals.org/cancerres/article-pdf/86/19/4755/3830682/can-25-5295.pdf by DKFZ - German Cancer Research Center user on 17 November 2026

Margo, the Annenberg Foundation, the Association Hubert Gouin Enfance et Cancer, the Fédération Enfants Cancers Santé, the Société Française de lutte contre les Cancers et les leucémies de l'Enfant et l'adolescent (SFCE), Les Bagouz à Manon, Les amis de Claire, La Ligue contre le Cancer, and the Fondation ARC pour la Recherche contre le Cancer (ARC). Funding was also obtained from INCa/SiRIC (grant INCa-DGOS-4654) and the PRTK2019-1-RT-02-ICR-1 grant. High-throughput sequencing was performed by the ICGex next-generation sequencing platform of the Institut Curie, supported by the grants ANR-10-EQPX-03 (Equipex) and ANR-10-INBS-09-08 (France Génomique Consortium) from the Agence Nationale de la Recherche ("Investissements d'Avenir" program), by the Canceropole Ile-de-France, and by the SiRIC-Curie program - SiRIC Grant "INCa-DGOS- 4654." Tumor sequencing data were also contributed from the MAPPYACTS protocol (clinicaltrial.gov: NCT02613962) and MICCHADO (NCT03496402). The authors thank Angela Bellini and Rachida Bouarich for their contributions. ACC (Alleanza Contro il Cancro), Italy: Funding was obtained under the following grant numbers: Associazione Bianca Garavaglia A/15/01N and A/18/01A. At IRCCS—Istituto Ortopedico Rizzoli, Experimental Oncology Laboratory, Bologna, Italy (Katia Scotlandi, Maria Cristina Manara, Lorena Landuzzi), the study was supported by the Innovative Medicines Initiative 2 Joint Undertaking ITCC P4 under grant agreement number 116064. Institute Gustave Roussy, France: At Gustave Roussy, the work was supported by grants from Fondation Gustave Roussy; Fédération Enfants Cancers et Santé; SFCE; Association AREMIG and Thibault BRIET; Parrainage médecin-chercheur of Gustave Roussy; INSERM; Canceropôle Ile-de-France; Ligue Nationale Contre le Cancer (Equipe labellisée); and Fondation ARC for the European projects ERA-NET on Translational Cancer Research (TRANSCAN 2) Joint Transnational Call 2014 (JTC 2014) "Targeting of Resistance in PEDiatric Oncology." Xentech, France: Patient-derived xenografts (PDX) were established with the Paris hospitals' network in France in collaboration with Sophie Branchereau, Pediatric Surgery Department, and Bicêtre Hospital, Le Kremlin-Bicêtre, France. RNA-seq and WGS FASTQ files of Xentech models were generated by Carolina Armengol, Childhood Liver Oncology Group, Health Sciences Research Institute Germans Trias i Pujol, Badalona; Liqin Zhu, Department of Pharmacy and Pharmaceutical Sciences, St. Jude Children's Research Hospital, and Memphis, TN. University of Zürich (UZH), Switzerland: At UZH, this work was supported by Swiss Cancer League projects KLS-5143-08-2020 and KFS-5422-08-2021, the Clinical Research Priority Program "Precision Heamatology/Oncology," the Childhood Cancer Research Foundation Switzerland, the Swiss National Science Foundation projects 3100-175558 and 10.000.473, the Balgrist Foundation, the ResOrtho Foundation, the FORCE Foundation, the Bryn Turner-Samuels Foundation, the Pierre Mercier Foundation, and the Sarcoma Foundation of America. The authors would like to express their sincere thanks to Jean-Pierre Bourquin, Beat Bornhauser, Irina Banzola, Stephanie Kasper, Willemijn Breunis, Daniel Müller, Sander Botter, Knut Husmann, and the Swiss Center for Musculoskeletal Biobanking. Experimental Pharmacology and Oncology (EPO), Germany: Funding sources/grant numbers: This project has received funding from the Innovative Medicines Initiative 2 Joint Undertaking ITCC P4 under grant agreement number 116064. Individuals/Organizations contributing to this work: Svetlana Gromova (technical assistance). Resources/Facilities: The project has been performed at the facilities and using resources of EPO Berlin-Buch GmbH. CHARITÉ, Germany: Funding sources: This project has received funding from the Innovative Medicines Initiative 2 Joint Undertaking ITCC P4 under grant agreement number 116064. This work was further supported by the DKTK and the parents' initiative at Charité KINDerLEBEN e.V. ICR, United Kingdom: At ICR, this work was supported by grants to Chris Jones from Cancer Research UK (DRCRPG-Nov21\100002), Abbie's Army, Cris Cancer Foundation, the Ollie Young Foundation, and Lucas' Legacy. The authors acknowledge NHS (National Health Service) funding to the ICR (Institute of Cancer Research) /Royal Marsden Hospital Biomedical Research Centre. At ICR, L. Chesler is financially supported by UK HEFCE/ICR support. The authors thank the patients, their families, and the staff at the Royal Marsden NHS Foundation Trust, Great Ormond Street Hospital for Sick Children, and the Royal Manchester Children's Hospital for their support in participation and donation of critical samples for this research. The authors would also like to thank Diana Carvalho for her contribution. L. Chesler and E.R. Tucker would personally like to acknowledge Dr. Paola Angelini and Mr. Tony Rogers for their vital help in the delivery of this project at ICR. FSJD (Fundació Sant Joan de Déu), Spain: At Hospital Sant Joan de Déu, the authors acknowledge the clinical fellows involved in the care of patients and the families of the children for donating the samples for research. The authors thank the Xarxa de Bancs de Tumors de Catalunya (sponsored by Pla Director d'Oncologia de Catalunya). MUW (Medizinische Universität Wien), Austria: University of Vienna: The project received funding from the City of Vienna Fund for Innovative Interdisciplinary Cancer Research (#21165). Charles University and University Hospital Motol, Czech Republic: The project received funding from the Ministry of Health of the Czech Republic, MH CZ–DRO (Ministry of Health of the Czech Republic – Institutional Support), University Hospital Motol, Prague, Czech Republic (00064203). Others: The authors thank the Pediatric Brain Tumor Research Fund Guild Run of Hope for their support in creating the PDX models described in this study. The authors thank Olaf Heidenreich, Elizabeth Schweighart, Jean-Pierre Bourquin, Beat Bornhauser, and Irina Banzola for their contributions to the ITCC-P4 consortium (Ministry of Health of the Czech Republic – Institutional Support).

Note

Supplementary data for this article are available at Cancer Research Online (http://cancerres.aacrjournals.org/).

Received November 19, 2025; revised April 4, 2026; accepted July 9, 2026; posted first July 10, 2026.

References

1. World Health Organization (WHO). Childhood cancer. 2025. Available from: https://www.who.int/news-room/fact-sheets/detail/cancer-in-children.
2. Gröbner SN, Worst BC, Weischenfeldt J, Buchhalter I, Kleinheinz K, Rudneva VA, et al. The landscape of genomic alterations across childhood cancers. Nature 2018;555:321–7. https://doi.org/10.1038/nature25480.
3. Ma X, Liu Y, Liu Y, Alexandrov LB, Edmonson MN, Gawad C, et al. Pan-cancer genome and transcriptome analyses of 1,699 paediatric leukaemias and solid tumours. Nature 2018;555:371–6. https://doi.org/10.1038/nature25795.
4. Capper D, Jones DTW, Sill M, Hovestadt V, Schrimpf D, Sturm D, et al. DNA methylation-based classification of central nervous system tumours. Nature 2018;555:469–74. https://doi.org/10.1038/nature26000.
5. Koelsche C, Schrimpf D, Stichel D, Sill M, Sahm F, Reuss DE, et al. Sarcoma classification by DNA methylation profiling. Nat Commun 2021;12:498. https://doi.org/10.1038/s41467-020-20603-4.
6. Pfister SM, Reyes-Múgica M, Chan JKC, Hasle H, Lazar AJ, Rossi S, et al. A summary of the inaugural WHO classification of pediatric tumors: transitioning from the optical into the molecular era. Cancer Discov 2022;12:331–55. https://doi.org/10.1158/2159-8290.CD-21-1094.
7. Sill M, Schrimpf D, Patel A, Sturm D, Jäger N, Sievers P, et al. Advancing CNS tumor diagnostics with expanded DNA methylation-based classification. Cancer Cell 2026;44:340–54.e2. https://doi.org/10.1016/j.ccell.2025.11.002.
8. van Tilburg CM, Pfaff E, Pajtler KW, Langenberg KPS, Fiesel P, Jones BC, et al. The pediatric precision oncology INFORM registry: clinical outcome and benefit for patients with very high-evidence targets. Cancer Discov 2021;11:2764–79. https://doi.org/10.1158/2159-8290.CD-21-0094.
9. Berlanga P, Pierron G, Lacroix L, Chicard M, Adam de Beaumais T, Marchais A, et al. The European MAPPYACTS trial: precision medicine program in pediatric and adolescent patients with recurrent malignancies. Cancer Discov 2022;12:1266–81. https://doi.org/10.1158/2159-8290.CD-21-1136.
10. Villani A, Davidson S, Kanwar N, Lo WW, Li Y, Cohen-Gogo S, et al. The clinical utility of integrative genomics in childhood cancer extends beyond targetable mutations. Nat Cancer 2023;4:203–21. https://doi.org/10.1038/s43018-022-00474-y.
11. Comitani F, Nash JO, Cohen-Gogo S, Chang AI, Wen TT, Maheshwari A, et al. Diagnostic classification of childhood cancer using multiscale transcriptomics. Nat Med 2023;29:656–66. https://doi.org/10.1038/s41591-023-02221-x.
12. Lau LMS, Khuong-Quang D-A, Mayoh C, Wong M, Barahona P, Ajuyah P, et al. Precision-guided treatment in high-risk pediatric cancers. Nat Med 2024;30:1913–22. https://doi.org/10.1038/s41591-024-03044-0.
13. Liu ITT, Kesselheim AS. The RACE act and pediatric trials of adult cancer drugs. Pediatrics 2024;154:e2024066920. https://doi.org/10.1542/peds.2024-066920.
14. Rokita JL, Rathi KS, Cardenas MF, Upton KA, Jayaseelan J, Cross KL, et al. Genomic profiling of childhood tumor patient-derived xenograft models to enable rational clinical trial design. Cell Rep 2019;29:1675–89.e9. https://doi.org/10.1016/j.celrep.2019.09.071.

Downloaded from aacrjournals.org/cancerres/article-pdf/86/19/4755/3830682/can-25-5295.pdf by DKFZ - German Cancer Research Center user on 17 November 2026

15. Brabetz S, Leary SES, Gröbner SN, Nakamoto MW, Şeker-Cin H, Girard EJ, et al. A biobank of patient-derived pediatric brain tumor models. Nat Med 2018;24:1752–61. https://doi.org/10.1038/s41591-018-0207-3.
16. Stewart E, Federico SM, Chen X, Shelat AA, Bradley C, Gordon B, et al. Orthotopic patient-derived xenografts of paediatric solid tumours. Nature 2017;549:96–100. https://doi.org/10.1038/nature23647.
17. Marques Da Costa ME, Zaidi S, Scoazec J-Y, Droit R, Lim WC, Marchais A, et al. A biobank of pediatric patient-derived-xenograft models in cancer precision medicine trial MAPPYACTS for relapsed and refractory tumors. Commun Biol 2023;6:949. https://doi.org/10.1038/s42003-023-05320-0.
18. Izumchenko E, Paz K, Ciznadija D, Sloma I, Katz A, Vasquez-Dunddel D, et al. Patient-derived xenografts effectively capture responses to oncology therapy in a heterogeneous cohort of patients with solid tumors. Ann Oncol 2017;28: 2595–605. https://doi.org/10.1093/annonc/mdx416.
19. Liu Y, Wu W, Cai C, Zhang H, Shen H, Han Y. Patient-derived xenograft models in cancer therapy: technologies and applications. Signal Transduct Target Ther 2023;8:160. https://doi.org/10.1038/s41392-023-01419-2.
20. Hidalgo M, Amant F, Biankin AV, Budinská E, Byrne AT, Caldas C, et al. Patient-derived xenograft models: an emerging platform for translational cancer research. Cancer Discov 2014;4:998–1013. https://doi.org/10.1158/2159-8290.CD-14-0001.
21. Joo KM, Kim J, Jin J, Kim M, Seol HJ, Muradov J, et al. Patient-specific orthotopic glioblastoma xenograft models recapitulate the histopathology and biology of human glioblastomas in situ. Cell Rep 2013;3:260–73. https://doi.org/10.1016/j.celrep.2012.12.013.
22. Stebbing J, Paz K, Schwartz GK, Wexler LH, Maki R, Pollock RE, et al. Patient-derived xenografts for individualized care in advanced sarcoma. Cancer 2014; 120:2006–15. https://doi.org/10.1002/cncr.28696.
23. Castillo-Ecija H, Pascual-Pasto G, Perez-Jaume S, Resa-Pares C, Vila-Ubach M, Monterrubio C, et al. Prognostic value of patient-derived xenograft engraftment in pediatric sarcomas. J Pathol Clin Res 2021;7:338–49. https://doi.org/10.1002/cjp2.210.
24. He F, Bandyopadhyay AM, Klesse LJ, Rogojina A, Chun SH, Butler E, et al. Genomic profiling of subcutaneous patient-derived xenografts reveals immune constraints on tumor evolution in childhood solid cancer. Nat Commun 2023; 14:7600. https://doi.org/10.1038/s41467-023-43373-1.
25. Akemi Kido L, Rodrigues Marusco M, Aparecida da Silva E, Do Carmo L, Beatriz Teodoro Borges A, Luz Torres Silva F, et al. Establishing a pediatric solid tumor PDX biobank for precision oncology research. Cancer Biol Ther 2025;26:2541974. https://doi.org/10.1080/15384047.2025.2541974.
26. Murphy B, Yin H, Maris JM, Kolb EA, Gorlick R, Reynolds CP, et al. Evaluation of alternative in vivo drug screening methodology: a single mouse analysis. Cancer Res 2016;76:5798–809. https://doi.org/10.1158/0008-5472.CAN-16-0122.
27. Jones DTW, Banito A, Grünewald TGP, Haber M, Jäger N, Kool M, et al. Molecular characteristics and therapeutic vulnerabilities across paediatric solid tumours. Nat Rev Cancer 2019;19:420–38. https://doi.org/10.1038/s41568-019-0169-x.
28. Li H. A statistical framework for SNP calling, mutation discovery, association mapping and population genetical parameter estimation from sequencing data. Bioinformatics 2011;27:2987–93. https://doi.org/10.1093/bioinformatics/btr509.
29. Uhrig S, Ellermann J, Walther T, Burkhardt P, Fröhlich M, Hutter B, et al. Accurate and efficient detection of gene fusions from RNA sequencing data. Genome Res 2021;31:448–60. https://doi.org/10.1101/gr.257246.119.
30. Merino DM, McShane LM, Fabrizio D, Funari V, Chen S-J, White JR, et al. Establishing guidelines to harmonize tumor mutational burden (TMB): in silico assessment of variation in TMB quantification across diagnostic platforms: phase I of the Friends of Cancer Research TMB Harmonization Project. J Immunother Cancer 2020;8:e000147. https://doi.org/10.1136/jitc-2019-000147.
31. Gao H, Korn JM, Ferretti S, Monahan JE, Wang Y, Singh M, et al. High-throughput screening using patient-derived tumor xenografts to predict clinical trial drug response. Nat Med 2015;21:1318–25. https://doi.org/10.1038/nm.3954.
32. Ackermann S, Cartolano M, Hero B, Welte A, Kahlert Y, Roderwieser A, et al. A mechanistic classification of clinical phenotypes in neuroblastoma. Science 2018;362:1165–70. https://doi.org/10.1126/science.aat6768.
33. Henrich K-O, Bender S, Saadati M, Dreidax D, Gartlgruber M, Shao C, et al. Integrative genome-scale analysis identifies epigenetic mechanisms of transcriptional deregulation in unfavorable neuroblastomas. Cancer Res 2016;76: 5523–37. https://doi.org/10.1158/0008-5472.CAN-15-2507.
34. Bonder MJ, Kasela S, Kals M, Tamm R, Lokk K, Barragan I, et al. Genetic and epigenetic regulation of gene expression in fetal and adult human livers. BMC Genomics 2014;15:860. https://doi.org/10.1186/1471-2164-15-860.
35. Calandrini C, Schutgens F, Oka R, Margaritis T, Candelli T, Mathijsen L, et al. An organoid biobank for childhood kidney cancers that captures disease and tissue heterogeneity. Nat Commun 2020;11:1310. https://doi.org/10.1038/s41467-020-15155-6.
36. Hassler MR, Pulverer W, Lakshminarasimhan R, Redl E, Hacker J, Garland GD, et al. Insights into the pathogenesis of anaplastic large-cell lymphoma through genome-wide DNA methylation profiling. Cell Rep 2016;17:596–608. https://doi.org/10.1016/j.celrep.2016.09.018.
37. Louis DN, Perry A, Wesseling P, Brat DJ, Cree IA, Figarella-Branger D, et al. The 2021 WHO classification of tumors of the central nervous system: a summary. Neuro Oncol 2021;23:1231–51. https://doi.org/10.1093/neuonc/noab106.
38. Sheffield NC, Pierron G, Klughammer J, Datlinger P, Schönegger A, Schuster M, et al. DNA methylation heterogeneity defines a disease spectrum in Ewing sarcoma. Nat Med 2017;23:386–95. https://doi.org/10.1038/nm.4273.
39. Qian W, Chen X, Sheng Y, Zhang L, Wang J, Song Z, et al. Tumor purity in preclinical mouse tumor models. Cancer Res Commun 2022;2:353–65. https://doi.org/10.1158/2767-9764.CRC-21-0126.
40. Eleveld TF, Oldridge DA, Bernard V, Koster J, Colmet Daage L, Diskin SJ, et al. Relapsed neuroblastomas show frequent RAS-MAPK pathway mutations. Nat Genet 2015;47:864–71. https://doi.org/10.1038/ng.3333.
41. Matthay KK, Maris JM, Schleiermacher G, Nakagawara A, Mackall CL, Diller L, et al. Neuroblastoma. Nat Rev Dis Primers 2016;2:16078. https://doi.org/10.1038/nrdp.2016.78.
42. Tirode F, Surdez D, Ma X, Parker M, Le Deley MC, Bahrami A, et al. Genomic landscape of Ewing sarcoma defines an aggressive subtype with co-association of STAG2 and TP53 mutations. Cancer Discov 2014;4:1342–53. https://doi.org/10.1158/2159-8290.CD-14-0622.
43. Tucker ER, Jiménez I, Chen L, Bellini A, Gorrini C, Calton E, et al. Combination therapies targeting ALK-aberrant neuroblastoma in preclinical models. Clin Cancer Res 2023;29:1317–31. https://doi.org/10.1158/1078-0432.CCR-22-2274.
44. Sun H, Cao S, Mashl RJ, Mo C-K, Zaccaria S, Wendl MC, et al. Comprehensive characterization of 536 patient-derived xenograft models prioritizes candidates for targeted treatment. Nat Commun 2021;12:5086. https://doi.org/10.1038/s41467-021-25177-3.
45. Chen X, Yang W, Roberts CWM, Zhang J. Author correction: developmental origins shape the paediatric cancer genome. Nat Rev Cancer 2024;24:513. https://doi.org/10.1038/s41568-024-00710-w.
46. Zhuo J, Su R, Tan W, Lian Z, Lu D, Xu X. The ongoing trends of patient-derived xenograft models in oncology. Cancer Commun (Lond) 2020; 40:559–63. https://doi.org/10.1002/cac2.12096.

Downloaded from aacrjournals.org/cancerres/article-pdf/86/19/4755/3830682/can-25-5295.pdf by DKFZ - German Cancer Research Center user on 17 November 2026